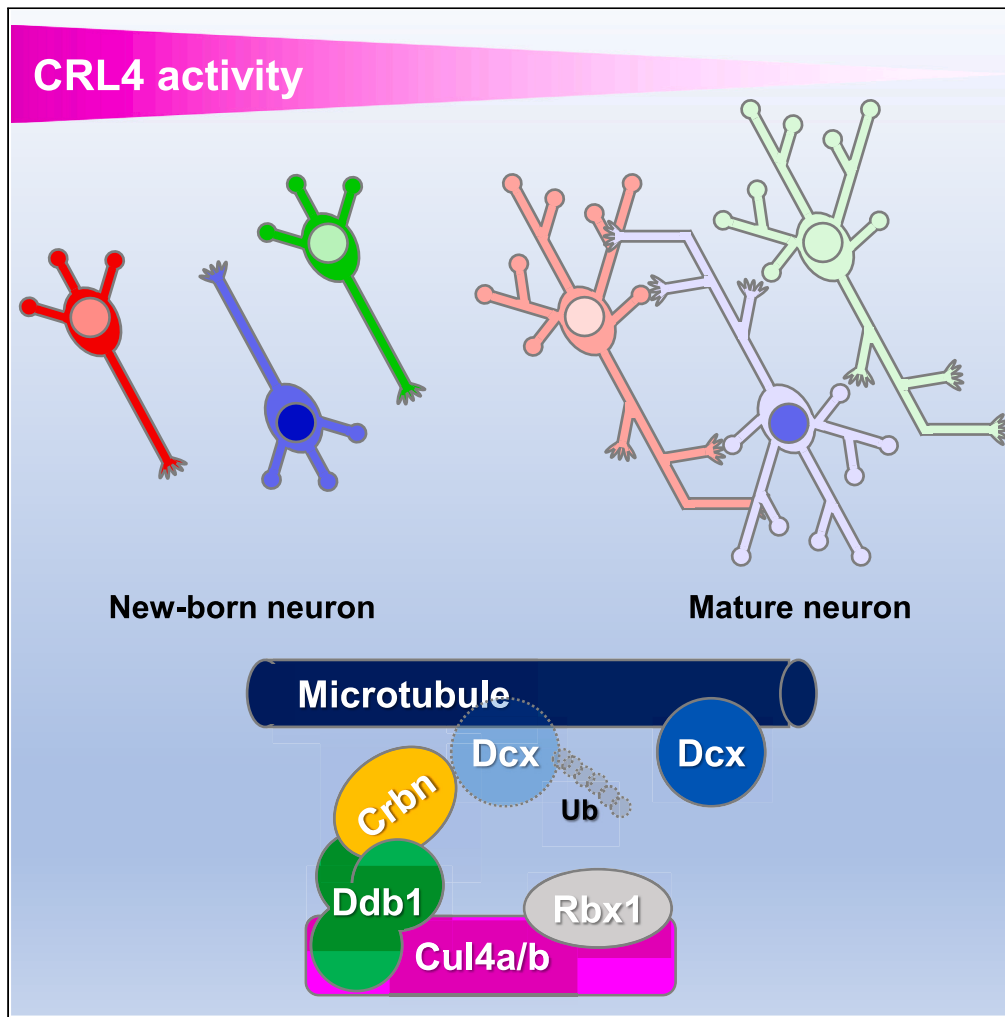


Article

Cullin-RING E3 ubiquitin ligase 4 regulates neurite morphogenesis during neurodevelopment



Tammy Shim, Jae Yeon Kim, WonCheol Kim, Yun-Il Lee, Bongki Cho, Cheil Moon

cbk34@dgist.ac.kr (B.C.)
cmoon@dgist.ac.kr (C.M.)

Highlights

CRL4 is upregulated in cytosolic compartment of developing neuron

NMDAR signaling influences CRL4 activity

CRL4 is vital for regulation of neuritogenesis

The CRL4-Crbn complex regulates Dcx stability, affecting microtubule dynamics



Article

Cullin-RING E3 ubiquitin ligase 4 regulates neurite morphogenesis during neurodevelopment

Tammy Shim,^{1,2} Jae Yeon Kim,³ WonCheol Kim,^{1,2} Yun-Il Lee,⁴ Bongki Cho,^{4,5,*} and Cheil Moon^{1,2,*}

SUMMARY

Neuritogenesis is crucial for establishing proper neuronal connections during brain development; its failure causes neurodevelopmental defects. Cullin-RING E3 ubiquitin ligase complexes participate in various neurodevelopmental processes by regulating protein stability. We demonstrated the regulatory function of Cullin-RING E3 ubiquitin ligase 4 (CRL4) in neurite morphogenesis during early neurodevelopment. Cul4a and Cul4b, the core scaffold proteins of CRL4, exhibit high expression and activation within the cytosol of developing neurons, regulated by neuronal stimulation through N-methyl D-aspartate (NMDA) receptor signaling. CRL4 also interacts with cytoskeleton-regulating proteins involved in neurite morphogenesis. Notably, genetic depletion and inhibition of cytosolic CRL4 enhance neurite extension and branching in developing neurons. Conversely, Cul4a overexpression suppresses basal and NMDA-enhanced neuritogenesis. Furthermore, CRL4 and its substrate adaptor regulate the polyubiquitination and proteasomal degradation of doublecortin protein. Collectively, our findings suggest that CRL4 ensures proper neurite morphogenesis in developing neurons by regulating cytoskeleton-regulating proteins.

INTRODUCTION

Neurons establish synaptic connections in a complex yet orderly manner, forming neural circuits for high-order brain function.¹ Developing neurons migrate to specific locations, build polarized structures, including axons and dendrites, and ultimately establish synapses. Within these neurodevelopmental processes, neuronal morphogenesis, particularly neuritogenesis, is a critical developmental event.² Spherical neural precursor cells initiate budding through asymmetric and focal accumulation of cortical actin.³ These budding extensions evolve into actin-rich filopodia and lamellipodia, ultimately maturing into microtubule-stabilized neurites categorized as axons or dendrites. These neurites extensively elongate and branch, resulting in complex synaptic connections. Therefore, neuritogenesis requires spatiotemporally dynamic changes in cytoskeletal structures, primarily orchestrating cellular morphological alterations.⁴

Actin filaments and microtubules, the main filamentous structures of neurites, are mainly formed through polymerization of ATP-bound globular actin and GTP-bound α/β -tubulin heterodimer, respectively, with the help of nucleation-promoting factors, including formins or the Arp2/3 complex for actin, and γ -tubulin ring complex for microtubules.⁵ The polymerized actin and α/β -tubulin heterodimer form a bundled structure by actin-bundling and microtubule-associated proteins. Then, they are transformed into ADP-bound actin and GDP-bound α/β -tubulin via hydrolysis, which depolymerizes them from actin filaments and microtubules.⁴ Dynamic equilibrium between polymerization and depolymerization determines structures of actin filaments and microtubules. Regulatory component proteins, including profilin and cofilin for actin filaments, and tau and stathmin for microtubules, can bidirectionally shift it. Additionally, cross-linking proteins such as doublecortin (Dcx) and drebrin, along with protein-trafficking motor proteins, including myosin and kinesin/dynein, play pivotal roles in coordinating actin filaments and microtubules.³ Consequently, genetic mutations in cytoskeletal components or cytoskeleton-regulating proteins are closely associated with neurodevelopmental disorders such as intellectual disability and autism spectrum disorders.^{2,6} Hence, the regulation of cytoskeletal proteins is essential for proper neuritogenesis.

The ubiquitination-proteasome system (UPS) has been proposed as a negative regulator of neuritogenesis.⁷ Smurf1, an E3 ubiquitin ligase, promotes neuritogenesis through ubiquitination-mediated degradation of RhoA, a regulator of actin dynamics.⁸ Recently, cullin-RING E3 ubiquitin ligases (CRLs), the predominant E3 ubiquitin ligase family in eukaryotes, have been implicated in neuritogenesis. CRL is a multi-protein complex formed by the core scaffold protein cullin, which acts as a platform for the E2 enzyme and substrates with the RING-finger protein Rbx1/2.^{9,10} Genetic depletion of cullin 3 (Cul3) in CRL3 induces abnormal accumulation of cytoskeletal proteins, which are involved in neuronal migration and dendritogenesis, resulting in social and cognitive impairments associated with autism spectrum disorder.^{11,12}

¹Department of Brain Sciences, DGIST, Daegu 42988, Republic of Korea

²Convergence Research Advanced Centre for Olfaction, DGIST, Daegu 42988, Republic of Korea

³Department of Neurology, University of California, San Francisco, CA 94143, USA

⁴Division of Biotechnology, DGIST, Daegu 42988, Republic of Korea

⁵Lead contact

*Correspondence: cbk34@dgist.ac.kr (B.C.), cmoon@dgist.ac.kr (C.M.)

<https://doi.org/10.1016/j.isci.2024.108933>



Similarly, Kelch-like 15 (Kihl15), a substrate adaptor for CRL3 implicated in X-linked intellectual disability, promotes destabilization of the Dcx protein, thereby inhibiting dendrite outgrowth.¹³ Mutations in human *CUL4B*, which encodes cullin 4b in CRL4, are also linked to X-linked intellectual disability.^{14,15} *Cul4b* knockout mice exhibit spatial learning defects and epileptic hypersensitivity with abnormal dendritic morphology in the interneurons of the hippocampus.¹⁶ However, the mechanism underlying the role of CRL4 in neurogenesis remains unknown.

In this study, we investigated the regulation of CRL4 and its involvement in neurological function during neurodevelopment to ascertain whether it serves as a regulatory component in neurogenesis during early neuronal development.

RESULTS

Cul4a and Cul4b are upregulated during early neuronal development

Unlike other CRLs, CRL4 comprises two distinct complexes with Cul4a or Cul4b, which are core scaffold proteins acting as paralog cullin proteins for CRL4.⁹ These two proteins share over 80% sequence similarity and, in conjunction with adaptor protein damage-specific DNA-binding protein 1 (Ddb1) and substrate-recognizing Ddb1/Cul4-associated factors (DCAFs), form the CRL4 complex. Thus, we examined the differential expression of Cul4a and Cul4b proteins during the developmental stage of cultured cerebral neurons.

Immunoblot data revealed that Cul4b and Ddb1 proteins substantially decreased from *in vitro* day 5 (DIV5) to DIV10, whereas Cul4a was consistently expressed until DIV17 (Figures 1A and 1B). Similarly, the level of *Cul4b* mRNA substantially decreased from DIV5 to DIV10, whereas *Cul4a* mRNA exhibited a slight increase (Figure S1). These results indicate that Cul4b is transcriptionally regulated during neuronal development.

Notably, both Cul4a and Cul4b revealed higher molecular weight shifts of approximately 10 kDa on immunoblots than their native forms (Figure 1A). Cullin proteins undergo neddylation, a covalent conjugation with neural-precursor-cell-expressed developmentally downregulated 8 (Nedd8), promoting CRL activation.¹⁷ Therefore, we examined whether the molecular weight shifts in Cul4a and Cul4b were caused by neddylation. Treatment with MLN4924, an inhibitor of Nedd8-activating enzyme E1 (Nae1), eliminated the Cul4a and Cul4b band shifts on the immunoblot. In contrast, treatment with CSN5i-3, an inhibitor of the deneddylating enzyme Nedd8 hydrolase Cop9 signalosome complex subunit 5 (Csn5), increased the band shift (Figure 1C), suggesting neddylation of Cul4a and Cul4b in neurons. The neddylated Cul4a levels did not change significantly, but native Cul4a increased on DIV10 compared with that on DIV5, leading to a significant decrease in the ratio of neddylated vs. native Cul4a (Figures 1A and D). Both neddylated and native Cul4b decreased on DIV10, with their ratio also decreasing (Figures 1A and E). These results suggest that CRL4 is highly expressed and activated during the early stage (DIV5) of neurodevelopment rather than at a later stage (DIV10), indicating its stage-specific developmental function.

We also performed immunocytochemistry to assess Cul4a and Cul4b. From DIV5 to DIV10, Cul4a immunoreactivity was evenly enriched in the nuclear and cytosolic compartments of neurons, colocalizing with Ddb1 immunoreactivity (Figure 1F). In contrast, the immunoreactivity of Cul4b, which possesses a nuclear localization signal (NLS) in the N-terminus,⁹ was highly enriched in the nucleus (Figure 1G). Notably, on DIV5, a significant fraction of Cul4b was accumulated in the cytosol, similar to Cul4a. According to the GenBank database, the rat *Cul4b* gene (gene ID: 361181) has three splicing-variant mRNAs: *Cul4b-1*, *-x1*, and *-x2*. *Cul4b-x2* protein lacks an N-terminal extension bearing an NLS sequence, unlike the other isoforms (Figure S2A). Concordantly, ectopically expressed *Cul4b-x2* was mostly present in the cytosol rather than the nucleus, whereas other isoforms were strongly accumulated in the nucleus with minimal cytosolic expression (Figure S2B). *Cul4b-1* and *-x2* transcript and protein levels were also high on DIV5 but significantly lower on DIV10 (Figures S2C and S2D). These data indicate that cytosolic Cul4b is primarily derived from the *Cul4b-x2* transcript. Additionally, subcellular fractionation data revealed that the level of cytosolic Cul4a and Cul4b was high on DIV5 with Ddb1 but decreased on DIV10 (Figures 1H and 1I).

Immunohistochemistry of rat brains revealed that Cul4a immunoreactivity displayed cytosolic expression with Ddb1 in the cortical plate of the cerebral cortex of the embryonic brain, where developing neurons primarily exist (Figure 1J). In the cerebral cortex layer V of the adult brain, which contains the cell bodies of mature neurons, Cul4a was still enriched in both the nucleus and cytosol with Ddb1. In contrast, Cul4b exhibited cytosolic localization in the cortical plate of the embryonic brain but revealed evident nuclear accumulation in the adult brain (Figure 1K), consistent with the immunocytochemistry data. Collectively, our findings suggest that CRL4 is highly expressed and activated in the cytosol of developing neurons (Figure 1L).

Neuronal activity controls CRL4 via N-methyl D-aspartate receptor signaling

Neuronal activity tightly regulates neurodevelopmental processes, including neurogenesis, polarization via axon/dendrite specification, and the final formation of synapses.^{18,19} Since more developed neurons exhibit higher neuronal activity and lower CRL4 activity, we hypothesized that neuronal activity may regulate CRL4. To investigate this, we stimulated mature neurons (DIV10) by transiently treating them with glutamate (Glu) (Figure 2A). The level of Ddb1 protein was not affected by Glu (Figures 2B and 2C). Total Cul4a significantly increased (Figures 2B and 2D), with the native form demonstrating a higher increase than the neddylated form (Figures 2B and 2E). The level of *Cul4a* mRNA also increased (Figure S3), indicating that Cul4a expression is transcriptionally upregulated by Glu, while its neddylation is downregulated.

Co-treatment with D-AP5, a competitive antagonist of the N-methyl D-aspartate receptor (NMDAR), did not significantly affect Glu-induced upregulation of total Cul4a (Figure 2D). However, D-AP5 further increased the level of neddylated, but not native, Cul4a, thus reversing the Glu-induced downregulation of neddylation (Figure 2E). D-AP5 also reversed the Glu-induced expression of *Cul4a* mRNA (Figure S3). Neither NBQX, an AMPA/kainate receptor antagonist nor LY341495 (LY), a metabotropic glutamate receptor antagonist, affected the expression and neddylation of Cul4a (Figures 2B–2E). Additionally, Glu induced nuclear accumulation of Cul4a along with Ddb1, which was

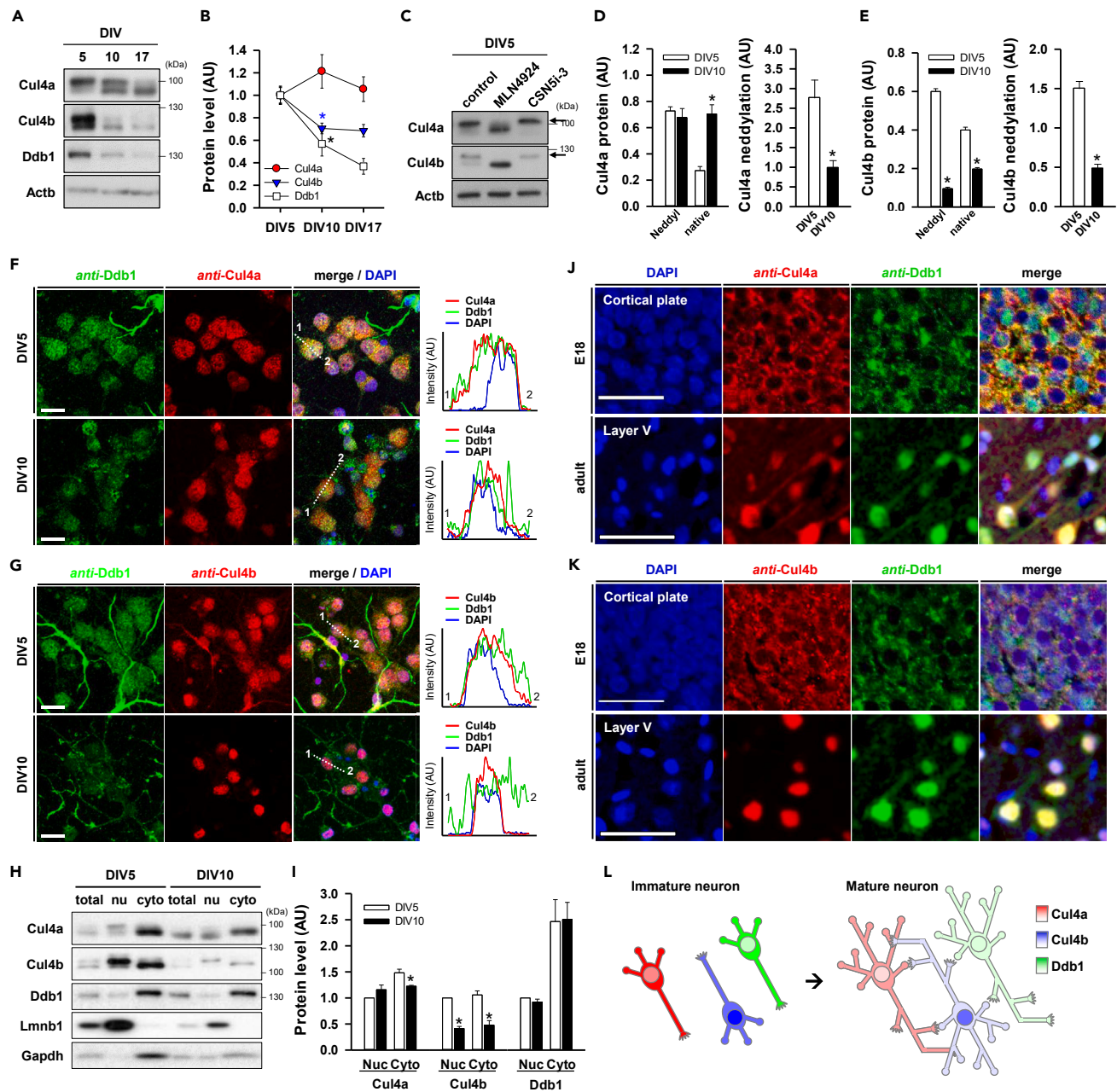


Figure 1. Expression of CRL4 during neuronal development

(A and B) Representative immunoblots (A) and relative levels normalized by Actb (B) of CRL4 proteins in cultured cerebral neurons ($n = 3$; $*p < 0.05$, DIV5 versus DIV10 by two-tailed unpaired t-test; Data are represented as mean \pm SEM.).

(C) Representative immunoblots of Cul4a and Cul4b in DIV5 neurons treated with or without MLN4924 or CSN5i-3 for 24 h. Arrows indicate the neddylated forms of Cul4a and Cul4b.

(D and E) The left graphs represent the portions of neddylated and native forms of Cul4a (D) and Cul4b (E) at DIV5 and DIV10. The graphs on the right show the ratio of neddylated versus native form ($n = 3$; $*p < 0.05$, DIV5 versus DIV10 by two-tailed unpaired t-test; Data are represented as mean \pm SEM.).

(F and G) Representative images of the immunocytochemistry of Cul4a (F) or Cul4b (G) with Ddb1 in DIV5 and DIV10 neurons (Scale bar, 10 μ m). The graphs on the right show the intensity of immunoreactivities of Cul4a or Cul4b with Ddb1 and DAPI in dotted lines (1–2).

(H and I) Representative immunoblots (H) and relative levels (I) of Cul4a, Cul4b, and Ddb1 in total, nuclear (nuc) and cytosolic (cyto) fractions of *in vitro* cultured neurons ($*p < 0.05$, DIV5 versus DIV10 by two-tailed unpaired t-test; Data are represented as mean \pm SEM.).

(J and K) Representative images for immunohistochemistry of Cul4a (J) or Cul4b (K) with Ddb1 in cortical plate of embryonic day 18 (E18) and cortical layer V of adult rat brains (Scale bar, 50 μ m).

(L) Graphic summary of cytosolic and nuclear expression of Cul4a, Cul4b, and Ddb1. The expression level is visualized by red, green, and blue intensity, respectively.

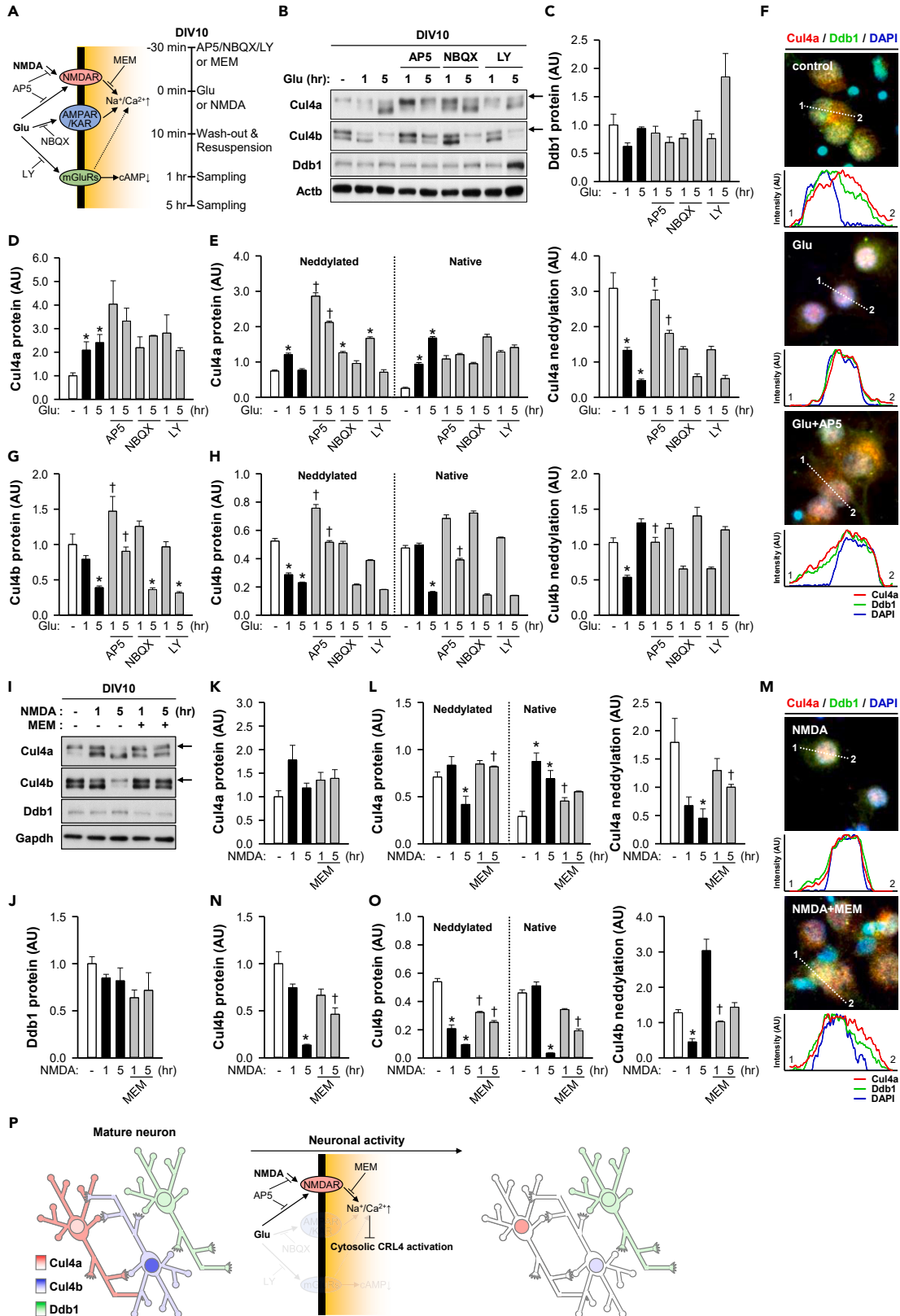


Figure 2. Expression and neddylation of Cul4a and Cul4b are controlled by neuronal activity

(A) Schematic diagram of experiment (Glu, glutamate; AP5, D-AP5; LY, LY341495; MEM, memantine, NMDAR, NMDA receptor; AMPAR, AMPA receptor; KAR, Kainate receptor; mGluRs, metabotropic glutamate receptors).

(B) Representative immunoblots of CRL4 proteins in DIV10 neurons stimulated by 25 μ M Glu for 10 min with or without pre- and post-treatments of antagonists of glutamate receptor (50 μ M AP5, 10 μ M NBQX, or 10 μ M LY). Arrows indicate the neddylated forms of Cul4a and Cul4b.

(C–E) The relative level of Ddb1 (C) and total Cul4a (D) is normalized by Actb. (E) Relative levels of neddylated, native forms and the neddylation ratio (neddylated versus native) of Cul4a ($n = 3$, $*p < 0.05$ to the no-treatment group, $\dagger p < 0.05$ to the glutamate-treatment group in the same treatment time by two-tailed unpaired t-test; Data are represented as mean \pm SEM.). (F) Representative images (upper panels) and relative intensities (below panels) of the immunocytochemistry of Cul4a and Ddb1 in neurons stimulated by glutamate with or without AP5. (G–H) The relative level of total Cul4b (G) is normalized by Actb. (H) Relative levels of neddylated, native forms and the neddylation ratio (neddylated versus native) of Cul4b ($n = 3$, $*p < 0.05$ to the no-treatment group, $\dagger p < 0.05$ to the glutamate-treatment group in the same treatment time by two-tailed unpaired t-test; Data are represented as mean \pm SEM.).

(I) Representative immunoblot of CRL4 proteins under 100 μ M NMDA stimulation with or without 10 μ M MEM. Arrows indicate the neddylated forms of Cul4a and Cul4b.

(J–L) The relative level of Ddb1 (J) and total Cul4a (K) is normalized by Gapdh. (L) Relative levels of neddylated, native forms and the neddylation ratio (neddylated versus native) of Cul4a ($n = 3$, $*p < 0.05$ to the no-treatment group, $\dagger p < 0.05$ to NMDA-treatment group in the same treatment time by two-tailed unpaired t-test; Data are represented as mean \pm SEM.). (M) Representative images of the immunocytochemistry of Cul4a and Ddb1 in neurons stimulated by NMDA with or without MEM. The below panels indicate relative intensities in the dotted line (1–2). (N–O) The relative level of total Cul4b (N) is normalized by Gapdh. (O) Relative levels of neddylated, native forms and the neddylation ratio (neddylated versus native) of Cul4b ($n = 3$, $*p < 0.05$ to the no-treatment group, $\dagger p < 0.05$ to NMDA-treatment group in the same treatment time by two-tailed unpaired t-test; Data are represented as mean \pm SEM.).

(P) Summary of change of expression, activity, and localization of Cul4a and Cul4b under neuronal activation.

suppressed by D-AP5 (Figure 2F). These data imply that the expression, neddylation, and cytosolic localization of Cul4a may be regulated by neuronal activation via NMDAR signaling.

Unlike Cul4a, levels of total, neddylated, and native Cul4b gradually decreased until 5 h after Glu treatment, along with a reduction in Cul4b neddylation (Figures 2B, 2G, and 2H); however, *Cul4b* mRNA expression levels were slightly increased (Figure S3). These data indicate that Glu-treated Cul4b has post-translational, rather than transcriptional, expression. D-AP5 efficiently reversed the Glu-induced reduction of total, neddylated, and native Cul4b, as well as the decrease in neddylation, but did not affect either NBQX or LY (Figures 2B, 2G, and 2H). These results suggest that Cul4b is also downregulated by neuronal activation.

We further examined whether NMDAR signaling directly regulates CRL4. NMDA stimulation did not affect the level of Ddb1 protein (Figures 2A, 2I, and 2J), whereas it induced the upregulation of native, but not neddylated, Cul4a, along with a reduction in neddylation, and nuclear accumulation of Cul4a, similarly to the Glu treatment (Figures 2I and 2K–2M). However, memantine (MEM), an ion channel blocker of NMDAR, completely reversed the changes in Cul4a expression and nuclear accumulation (Figures 2I and 2K–2M). Cul4b levels were gradually reduced by NMDA over 5 h, and MEM efficiently reversed this effect (Figures 2I, 2N, and 2O). These results indicate that cytosolic CRL4 is downregulated by a cation influx via NMDAR during neuronal activation (Figure 2P). Considering that cytosolic expression and neddylation of Cul4a and Cul4b are higher in immature than mature neurons, we postulated that CRL4 may function in the cytosol during the early neurodevelopmental stage.

CRL4 interacts with cytoskeleton-organizing proteins

To explore novel functions of CRL4 in neurodevelopment, we immunoprecipitated CRL4-interacting proteins using Cul4a and Cul4b antibodies from cultured neuronal lysates and performed LC-MS/MS analysis on proteins enriched in SDS-PAGE stained with Coomassie blue (Figures 3A and 3B; Table S1, Data S1, S2, S3, and S4). Cul4a and Cul4b antibody immunoprecipitants exhibited specific binding proteins, unlike the GFP antibody used as a control (Figure S4). Although Cul4a- and Cul4b-interacting proteins highly overlapped, there was evidence of some unique interacting proteins (Table S1), implying substantial functional redundancy between Cul4a and Cul4b. Gene ontology (GO) clustering analysis revealed that the pool size and GO terms of Cul4a/b-interacting proteins on DIV5 were smaller than those on DIV10, suggesting the multifaceted role of CRL4 during neurodevelopment. Notably, we identified actin-filament protein (Actb), microtubule-associated proteins (Dcx and Dbn1), Sema3A signaling proteins (Crmp1 and Dpysl2/3/5), myosin proteins (Myh10 and Myo5a), and spectrin proteins (Sptan1 and Sptbn1) as common between Cul4a and Cul4b (Figures 3C and 3D). These proteins play crucial roles in neuronal morphogenesis, including axon guidance and projection, by regulating cytoskeletal organization (Figures 3C–3E). *In vitro* cultured hippocampal or cerebral neurons undergo axon specification and extension with short dendrites on DIV4.²⁰ Therefore, we hypothesized that CRL4 may be involved in morphogenesis during neurodevelopment.

Cytosolic CRL4 restricts axonal extension and branching in early neurodevelopment

To examine the impact of CRL4 on neuritogenesis, we depleted *Cul4a* or *Cul4b* expression on DIV2 using the CRISPR-Cas9 knockout system (Figure S5A). On DIV4, we observed that GFP-expressing *Cul4a*-knockout (sgCul4a) and *Cul4b*-knockout (sgCul4b) neurons had depleted immunoreactivities of Cul4a and Cul4b (Figure S5B), and they displayed longer and more complex neurites compared with that in the control (sgLacZ) neurons (Figure 4A). Sholl analyses revealed that sgCul4a and sgCul4b increased the complexity of distal axons and proximal dendrites (Figure 4B). In addition, the length of total neurites, axons, and dendrites was significantly increased by sgCul4a (total, $p < 0.001$ vs. sgLacZ by Mann-Whitney rank-sum test; axon, $p = 0.032$; dendrite, $p < 0.001$), or sgCul4b (total, $p = 0.023$; dendrite, $p = 0.001$)

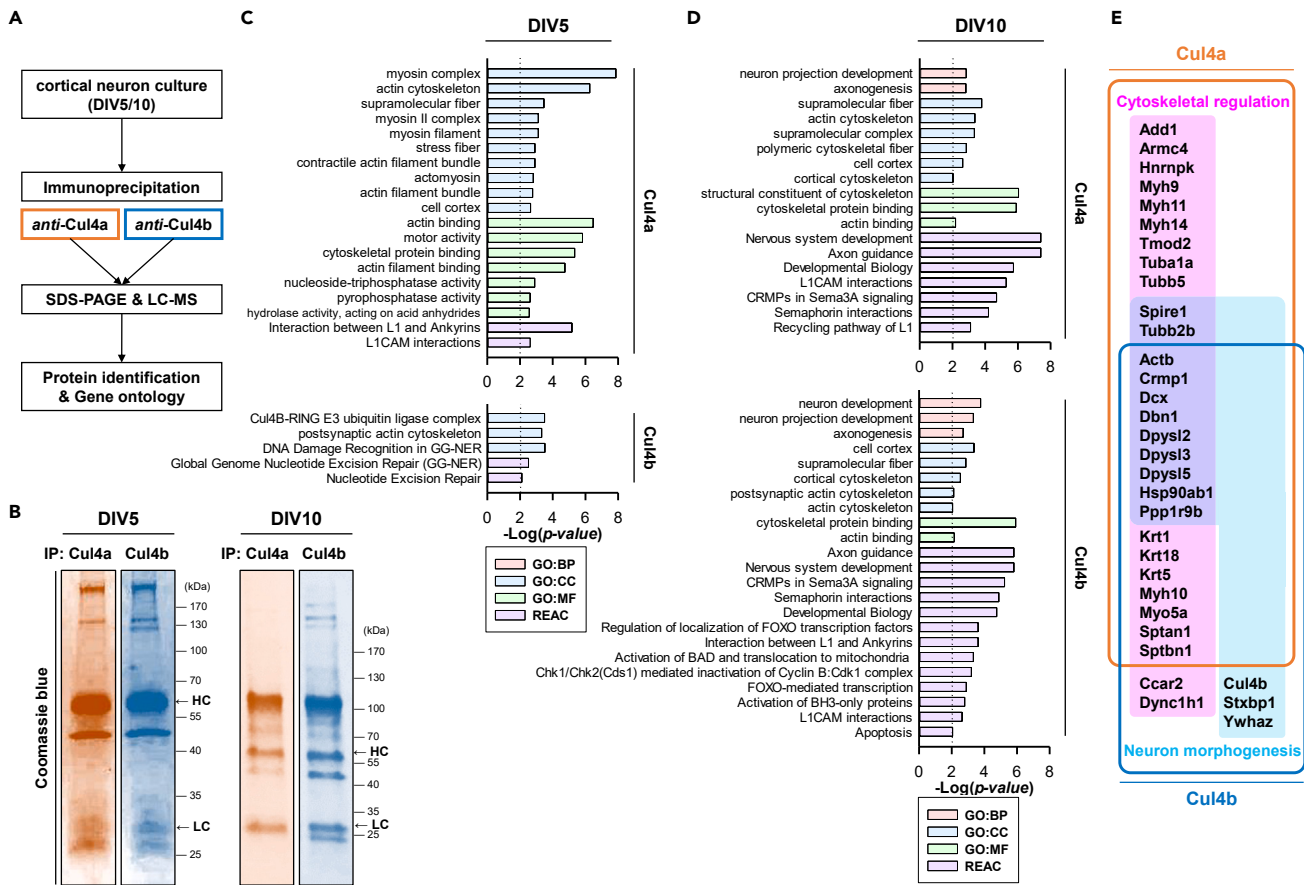


Figure 3. CRL4 interacts with cytoskeletal proteins in developing neurons

(A) Experimental strategy for identification of Cul4a- and Cul4b-binding proteins.

(B) Cul4a- and Cul4b-immunoprecipitates from lysates of DIV5 and DIV10 neurons. Proteins loaded onto polyacrylamide gel were stained by Coomassie blue. HC and LC indicate heavy and light chains of immunoprecipitated anti-Cul4a- and anti-Cul4b antibodies, respectively.

(C and D) Gene ontology and Reactome analyses of Cul4a- and Cul4b-binding proteins. Top GO:BP (biological process), GO:CC (cellular component), GO:MF (molecular function), and REAC (reactome) having $-\log(p)$ value was over 2 of DIV5 (C) and DIV10 (D) neurons.

(E) Selected list of proteins involved in cytoskeletal regulation and/or neuronal morphogenesis in the proteome of DIV10 neuron. Proteins within the pink box are related to cytoskeleton regulation, and those in the blue box are related to neuronal morphogenesis.

(Figures 4C and 4D). Number of neurites also was increased by sgCul4a (total, $p < 0.001$; axon, $p = 0.001$; dendrite, $p < 0.001$), or sgCul4b (total, $p < 0.001$; axon, $p < 0.001$; dendrite, $p < 0.001$) (Figures 4E and 4F).

Additionally, we investigated the effect of inhibiting endogenous CRL4 by overexpressing the dominant-negative Cul4a (DN-Cul4a) or Cul4b (DN-Cul4b) mutant, lacking cullin, Rbx1/2-binding, and neddylation domains, effectively sequestering Ddb1 from CRL4²¹ (Figure 5A). Flag-tagged DN-Cul4a and DN-Cul4b primarily localized to the cytosol and nucleus, respectively (Figures 5B and 5C), indicating substantial cytosolic and nuclear inhibition, respectively. Notably, DN-Cul4a-expressing neurons exhibited longer and more complex neurites than control neurons, whereas DN-Cul4b-expressing neurons did not exhibit evident morphological changes (Figure 5D). Sholl analyses revealed that DN-Cul4a increased the complexity of distal axons and proximal dendrites, whereas DN-Cul4b exhibited minimal increases, mainly in the dendrites (Figure 5E). Moreover, DN-Cul4a significantly increased the length of neurites, especially axons, but not dendrites (total, $p = 0.039$ vs. con by Mann-Whitney rank-sum test; axon, $p = 0.040$) (Figures 5F and 5G). DN-Cul4a also increased the number of neurites, particularly dendrites, with a minor effect on dendrite branching (total, $p = 0.004$; dendrite, $p = 0.030$) (Figures 5A–5F).

Conversely, we overexpressed Cul4a and Cul4b with Ddb1 on DIV2 (Figure 6A). The overexpressed Cul4a primarily localized in the cytosol, whereas Cul4b with an NLS sequence was mainly found in the nucleus with minimal cytosolic expression (Figures 6B and 6C). Cul4a overexpression likely led to less complex neurites, especially axons, compared with that in the control group (Figures 6D and 6E), significantly shortening the length of neurites (total, $p = 0.016$ – 0.039 vs. Mock by Mann-Whitney rank-sum test; axon, $p = 0.054$; dendrite, $p = 0.014$) (Figures 6F and 6G), and decreasing axon branching (total, $p = 0.014$; axon, $p = 0.003$) (Figures 6H and 6I). In contrast, nucleus-localized Cul4b did not exert a significant effect on neurite morphology (Figures 6A–6I). These results suggest that cytosolic CRL4 regulates the morphogenesis of neurites during early neurodevelopment.

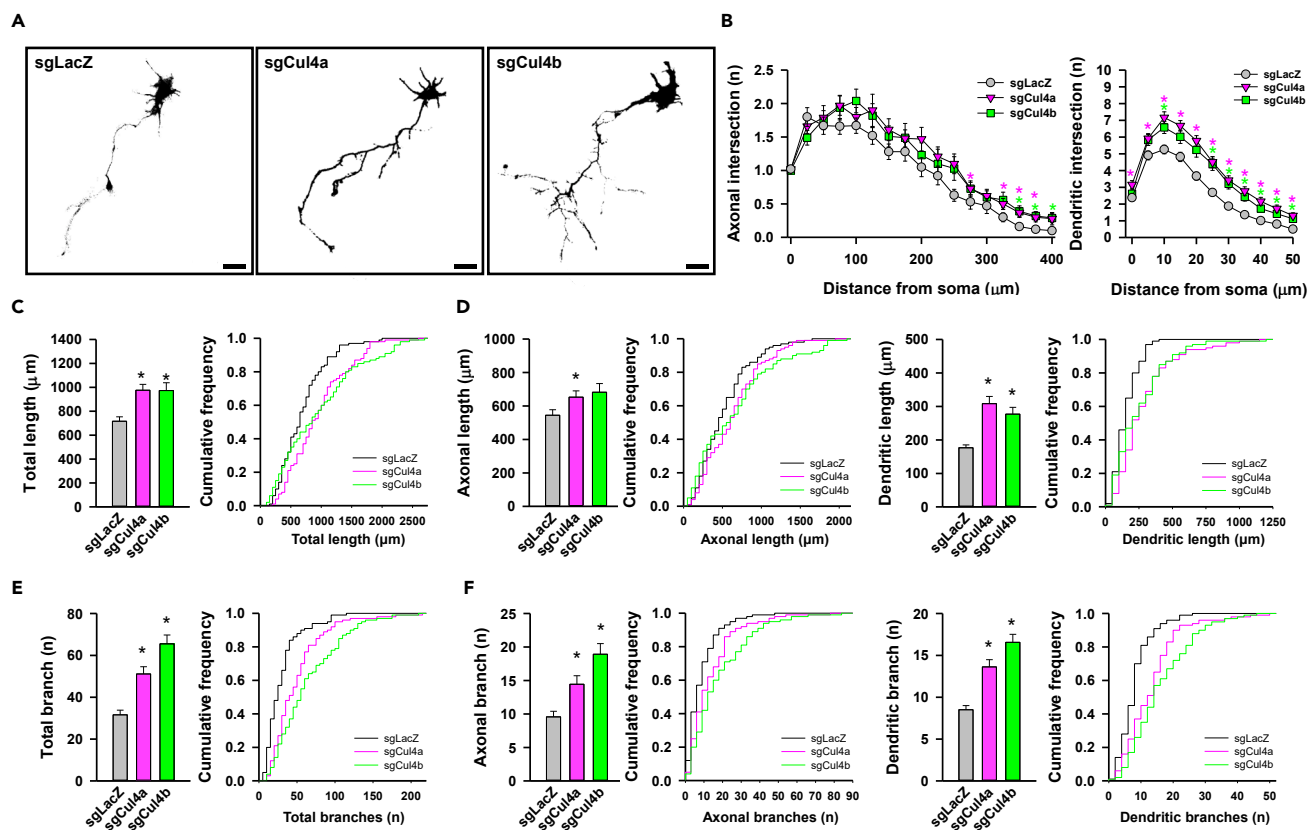


Figure 4. Genetic depletion of CRL4 induces neurite extension and branching in early neuronal development

(A) Representative images of the morphology of DIV4 neurons expressing the sgLacZ, sgCul4a, or sgCul4b (Scale bar, 30 μm).

(B) Sholl analyses of axon and dendrite. The number of intersections between neurites and concentric shells having 25 or 5 μm intervals (n = 100, *p < 0.05 to control group by Mann-Whitney rank-sum test; Data are represented as mean ± SEM).

(C–F) Average (left panels) and cumulative frequency (right panels) of length (C) and branch number (E) of total neurite, and length (D) and branch number (F) of axon/dendrite (n = 100, *p < 0.05 to control group by Mann-Whitney rank-sum test; Data are represented as mean ± SEM).

CRL4 antagonizes NMDA-induced neurite extension

NMDAR signaling plays a vital role in axonal and dendritic formation, outgrowth, and branching.^{22–25} Given that NMDAR activation down-regulates CRL4 in mature neurons (Figure 2), we explored its impact on CRL4 in immature neurons, which exhibit a lower calcium response to NMDA than mature neurons.²⁴ Notably, prolonged exposure to high concentration of NMDA (100 μM), which is non-toxic to immature neurons,^{24,26} did not influence the protein levels of Cul4a, Cul4b, or Ddb1 on DIV5 (Figures 7A and 7B). However, NMDA significantly increased Cul4b neddylation (Figures 7A and C).

We also examined the role of CRL4 in NMDAR-mediated neuronal morphogenesis. Similar to a previous report,²⁵ treatment with 1 μM NMDA substantially elongated total and axonal neurite length, significantly enhancing axon complexity without additional neurite branching (Figures 7D, 7E, and 7G–7J). However, overexpression of Cul4a or Cul4b effectively inhibited NMDA-induced neurite extension and complexity in both total neurites and axons (Figures 7D and 7F–7H). As CRL4 activity does not correlate with NMDA in immature neurons, our findings suggest that CRL4 inhibits NMDA-induced axonal extension and complexity through an NMDAR-independent mechanism.

CRL4-Crnb complex controls the stability of Dcx protein via UPS

Dcx plays a crucial role in axon and dendrite morphogenesis during neurodevelopment by stabilizing microtubules and regulating actin filaments.^{27–30} The stability of Dcx is post-translationally regulated by UPS, which is mediated by E3 ligases, including CRL3 and Mdm2.^{13,31} Therefore, we hypothesized that CRL4 might also control Dcx stability. Through immunoblotting following immunoprecipitation, we confirmed that a small fraction of Dcx interacts with Cul4a and Cul4b in DIV4 neurons (Figure 8A). On DIV10, when cytosolic Cul4b was not expressed (Figures 1A and 1G), only Cul4a, not Cul4b, interacted with Dcx (Figure 8B). Immunocytochemistry data revealed that Dcx immunoreactivity colocalized with Cul4a or Cul4b in proximal neurites near the soma of DIV4 neurons (Figure S6). Furthermore, proximity ligation assay (PLA) revealed the interaction between Dcx and CRL4. Notably, the amplified PLA

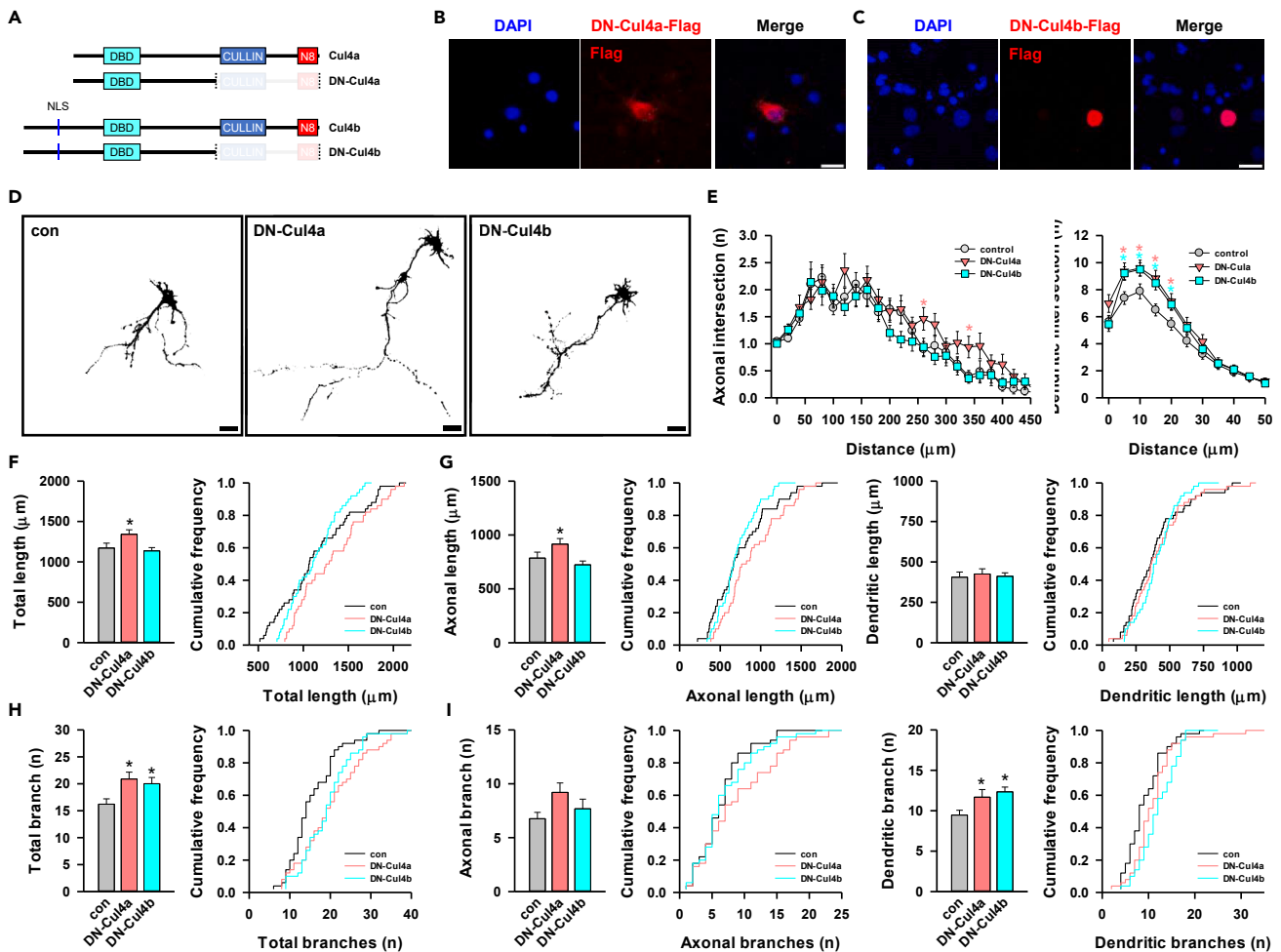


Figure 5. Inhibition of cytosolic CRL4 enhances neurite morphogenesis in developing neurons

(A) Structural domains of DN-Cul4 and DN-Cul4b.

(B and C) Immunofluorescence images of DN-Cul4a-Flag (B) and DN-Cul4b-Flag (C) in transfected DIV4 neurons (Scale bar, 20 μ m).

(D) Representative images of the morphology of DIV4 neurons expressing the control vector, DN-Cul4a or DN-Cul4b (Scale bar, 30 μ m).

(E) Sholl analyses of axon and dendrite. The number of intersections between neurites and concentric shells having 20 or 5 μ m intervals ($n = 50$, * $p < 0.05$ to control group by one-way ANOVA on ranks using Dunnett's Method; Data are represented as mean \pm SEM.).

(F–I) Average (left panels) and cumulative frequency (right panels) of length (F) and branch number (G) of total neurite, and length (H) and branch number (I) of axon/dendrite ($n = 50$, * $p < 0.05$ to control group by one-way ANOVA on ranks using Dunnett's Method; Data are represented as mean \pm SEM.).

signals of Cul4a-Dcx and Cul4b-Dcx displayed a punctate pattern on Tau-labeled proximal and distal axon segments, as well as around the soma (Figure 8C). These results indicate that cytosolic Cul4a and Cul4b specifically associate with a subset of Dcx in neurites.

Next, to investigate the mechanisms by which CRL4 affects Dcx protein, we overexpressed DN-Cul4a and/or DN-Cul4b in PC12 cells, which endogenously express Dcx.³² The level of DN-Cul4b was significantly higher than that of DN-Cul4a, although bi-cistronic GFP expression indicated a similar level, suggesting that DN-Cul4b is more stable than DN-Cul4a (Figure 8D). Concordantly, both DN-Cul4a and DN-Cul4b significantly increased the levels of Dcx protein, and their co-expression further elevated Dcx protein levels (Figure 8D). These data indicate that CRL4 negatively regulates Dcx expression.

To further investigate whether the UPS is involved in CRL4-mediated Dcx regulation, we used MG132, an inhibitor of the proteasome that accumulates high-molecular-weight polyubiquitinated proteins on SDS-PAGE gels. MG132 increased the levels of Dcx with high molecular shifts (Figure 8E), indicating that, as previously reported, Dcx is polyubiquitinated and degraded by the UPS.³³ Notably, the overexpression of Cul4a or Cul4b substantially increased the levels of polyubiquitinated Dcx compared with that in the control. Furthermore, co-immunoprecipitation data revealed that polyubiquitinated Dcx was detected in both Dcx and ubiquitin immunoprecipitants, and overexpression of Cul4a or Cul4b increased the levels of polyubiquitinated Dcx compared with that in the control group (Figure 8F). These results suggest that the level of Dcx is controlled by CRL4-UPS signaling.

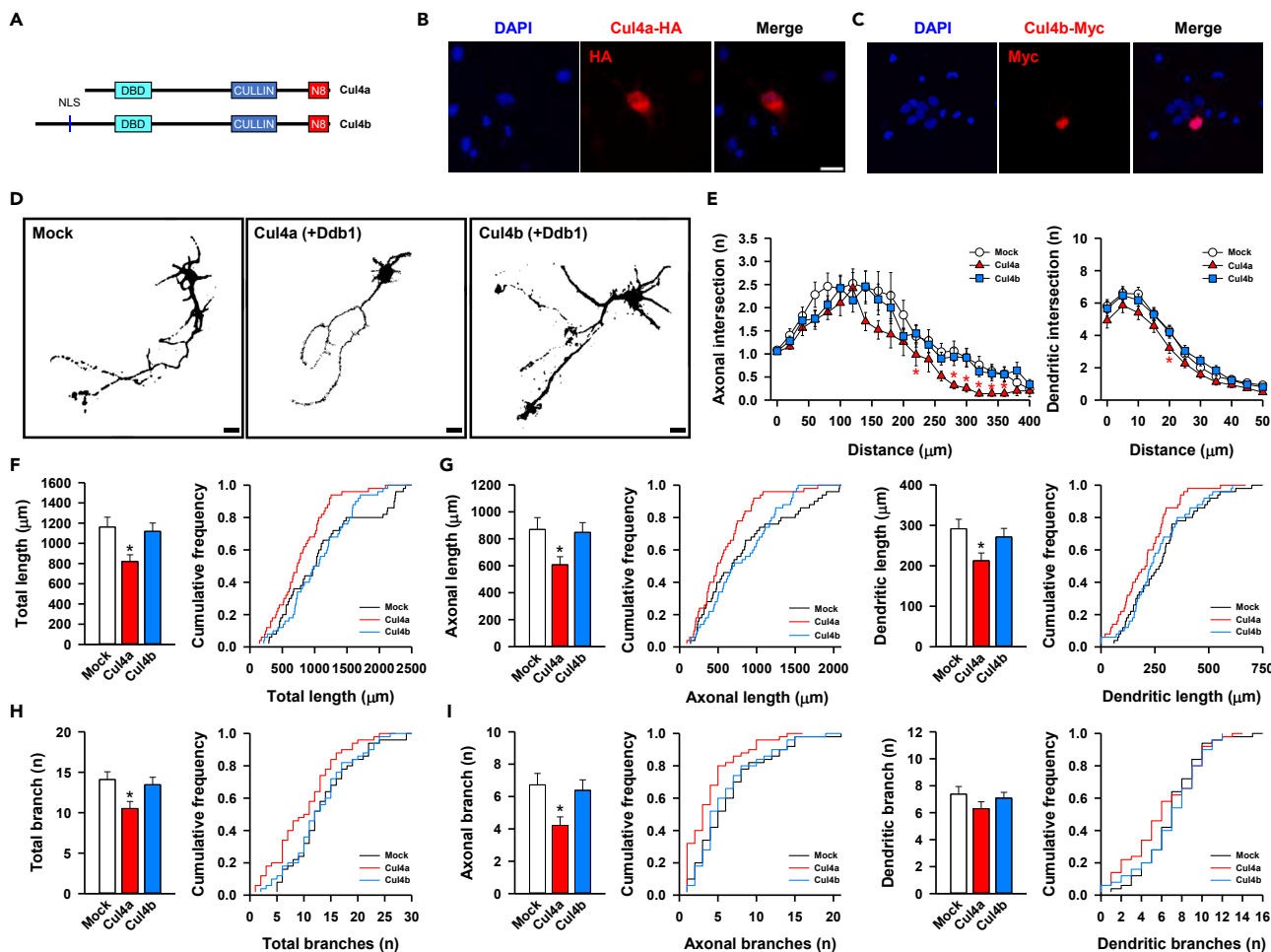


Figure 6. Overexpression of Cul4a suppresses neurite extension and branching in developing neurons

(A) Structural domains of Cul4a and Cul4b; NLS, nuclear localizing signal; DBD, Ddb1-binding domain; CULLIN, cullin homology domain; N8, Neddylaton domain. (B and C) Immunofluorescence images of Cul4a-HA (B) and Cul4b-Myc (C) in transfected DIV4 neurons.

(D) Representative images of the morphology of DIV4 neurons expressing control vector, Cul4a+Ddb1 or Cul4b+Ddb1 with GFP (Scale bar, 30 μ m).

(E) Sholl analyses of axon and dendrite. The number of intersections between neurites and concentric shells having 20 or 5 μ m interval ($n = 50$, * $p < 0.05$ to Mock group by one-way ANOVA on ranks using Dunnett's Method; Data are represented as mean \pm SEM.).

(F–I) Average (left panels) and cumulative frequency (right panels) of length (F) and branch number (G) of total neurite, and length (H) and branch number (I) of axon/dendrite ($n = 50$, * $p < 0.05$ to control group by one-way ANOVA on ranks using Dunnett's Method; Data are represented as mean \pm SEM.).

Given that DCAF associates with Ddb1 and is required to recruit the substrate to CRL4,⁹ we screened DCAF for the association between CRL4 and Dcx. Through a literature survey, open-source tissue, and intracellular expression data in the brain,^{34,35} we selected cereblon (Crbn) as a putative DCAF for Dcx. Crbn is associated with autosomal recessive intellectual disability.³⁶ Its immunoreactivity was highly enriched in the cytosol around the soma and neurites of cultured neurons (Figure S7A), as previously reported.³⁷ PLA signaling between Crbn and Ddb1 exhibited a punctate pattern on Map2-labeled neurites (Figure S7B). These data imply that Crbn may associate with CRL4 in neurons. Notably, the PLA signal between Dcx-Crbn also displayed a punctate pattern on phalloidin-labeled actin filaments in neurites, similar to that of Dcx-Cul4a and Dcx-Cul4b (Figure 8G). These results suggest that the CRL4-Crbn complex associates with Dcx in neurites.

To investigate the mechanisms by which Crbn contributes to CRL4-mediated regulation of Dcx protein, we genetically perturbed Crbn expression. Overexpression of Crbn significantly reduced Dcx levels (Figures S7C and S7D). Furthermore, overexpression of Cul4a+Ddb1 or Cul4b+Ddb1, as well as co-expression of Crbn, significantly decreased the level of Dcx (Figure 8H). In contrast, genetic depletion of Crbn (sgCrbn) achieved using the CRISPR-Cas9 knockout system efficiently reversed the reduction of Dcx levels upon overexpression of Cul4a+Ddb1 or Cul4b+Ddb1 (Figure 8I). Collectively, our findings suggest that CRL4 regulates the stability of Dcx via Crbn.

Next, we examined the mechanisms by which Crbn-CRL4 complex-mediated Dcx regulation impacts microtubule dynamics. The level of acetylated α -Tubulin, which is enriched in stable microtubules,³⁸ was reduced by overexpression of Cul4a and Cul4b along with Ddb1, and

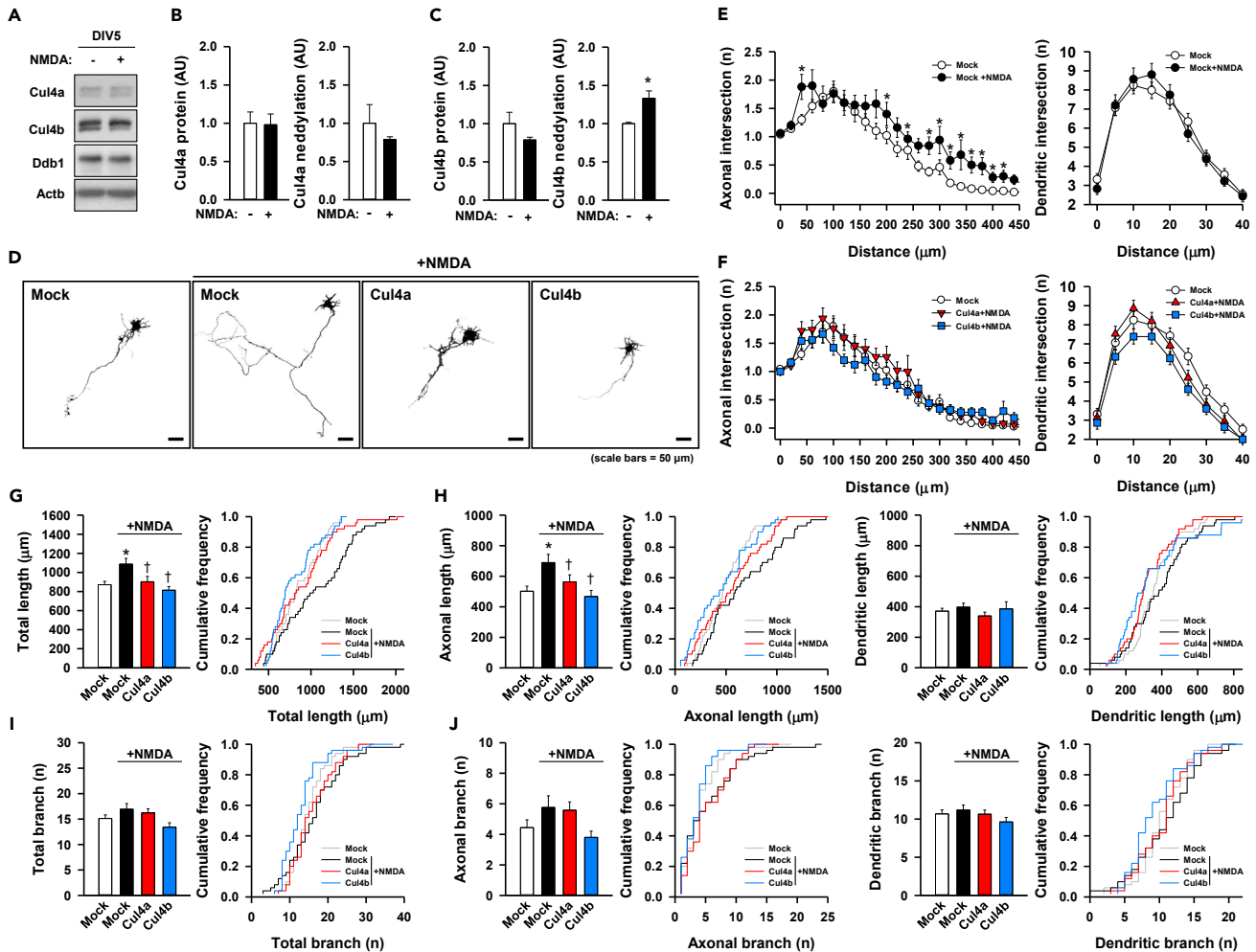


Figure 7. Overexpression of Cul4a or Cul4b abolishes NMDA-induced axonal extension

(A) Immunoblot of CRL4 proteins under the 100 μ M NMDA treatment for 24 h in DIV5 neurons.

(B and C) Quantification of relative protein level and neddylation ratio of Cul4a (B) and Cul4b (C) normalized by Actb level ($n = 3$, $*p < 0.05$ to no-NMDA group by two-tailed unpaired t-test; Data are represented as mean \pm SEM.).

(D) Representative images of the morphology of DIV4 neurons overexpressing Mock, Cul4a+Ddb1, or Cul4b+Ddb1 with or without 1 μ M NMDA for 48 h (Scale bars, 50 μ m).

(E) Sholl analyses of axon and dendrite of Mock-expressing neurons with or without NMDA. Average of intersections between neurites and concentric shells having 20 or 5 μ m interval ($n = 50$, $*p < 0.05$ to no-NMDA group by Mann-Whitney rank-sum test; Data are represented as mean \pm SEM.).

(F) Sholl analyses of axon and dendrite of Mock with no-NMDA, Cul4a+Ddb1 with NMDA, or Cul4b+Ddb1 with NMDA.

(G–J) Average (left panels) and cumulative frequency (right panels) of length (G) and branch number (H) of total neurite, and length (I) and branch number (J) of axon/dendrite. ($n = 50$, $*p < 0.05$ to no-NMDA group by Mann-Whitney rank-sum test; $\dagger p < 0.05$ to Mock+NMDA group by one-way ANOVA on ranks using Dunnett's Method; Data are represented as mean \pm SEM.).

this reduction was exacerbated by co-expression of Crbn (Figure 8J). Conversely, DN-Cul4b or DN-Cul4a+DN-Cul4b increased the level of acetylated α -Tubulin (Figure 8K). These results indicate that CRL4 regulates microtubule stabilization. Collectively, our findings suggest that CRL4 regulates neurite morphogenesis during the neurodevelopmental stage by restricting Dcx-mediated microtubule stabilization (Figure 8L).

DISCUSSION

This study demonstrated that cytosolic CRL4 plays a neuromorphogenic role in neurodevelopment. Cul4a, Cul4b, and Ddb1, the primary components of CRL4, are highly expressed in the cytosolic compartment of developing neurons. Cul4a predominantly localizes to the cytosolic compartment, whereas Cul4b tends to accumulate in the nucleus despite their high protein sequence identity and functional redundancy.⁹ This difference may be attributed to the NLS-bearing N-terminal extension of Cul4b. Notably, our findings revealed stage-specific

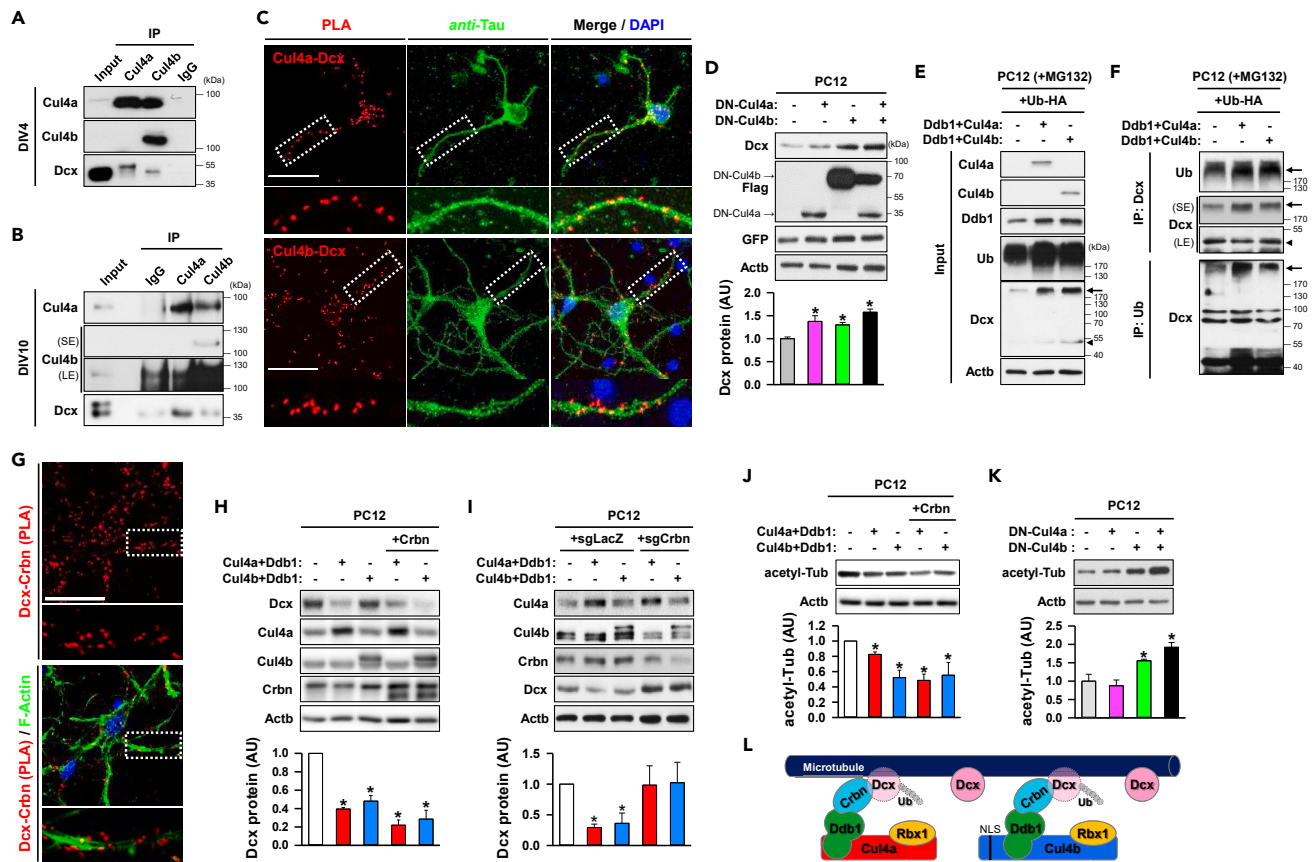


Figure 8. CRL4 regulates the protein level of Dcx

(A and B) Immunoblots of CRL4 and Dcx proteins from Cul4a- and Cul4b-immunoprecipitated DIV5 (A) and DIV10 neurons (B). (C) Representative images of the PLA signals of Cul4a and Cul4b with Dcx and immunolabeled signal of Tau in DIV2 neurons (Scale bar, 30 μ m). (D) Immunoblots and relative levels of Dcx protein normalized by the Actb level of DN-Cul4a and/or DN-Cul4b overexpressed PC12 cells (n = 4; *p < 0.05 to control group by two-tailed unpaired t-test; Data are represented as mean \pm SEM). (E and F) Immunoblots of input (E) and immunoprecipitants by Dcx and Ubiquitin (Ub) (F) in control, Ddb1+Cul4a- Ddb1+Cul4b-expressing PC12 cells treated by MG132. Arrows and arrowheads indicate high-molecularly shifted and native Dcx, respectively. (G) Representative images of the PLA signals between Dcx and Crbn with phalloidin-labeled actin-filament in DIV4 neurons (Scale bar, 30 μ m). (H) Immunoblots and relative levels of Dcx protein normalized by the Actb level in Cul4a- or Cul4b-overexpressing PC12 cells with or without Crbn (n = 3; *p < 0.05 to Mock group by two-tailed unpaired t-test; Data are represented as mean \pm SEM). (I) Immunoblot and relative levels of Dcx protein normalized by the Actb level in Cul4a- or Cul4b-overexpressing PC12 cells with sgLacZ or sgCrbn (n = 3; *p < 0.05 to Mock group by two-tailed unpaired t-test; Data are represented as mean \pm SEM). (J and K) Immunoblots and relative levels of acetylated α -Tubulin (acetyl-Tub) normalized by the Actb level in Cul4a+Ddb1- or Cul4b+Ddb1-overexpressing PC12 cells with or without Crbn (J) (n = 3; *p < 0.05 to empty vector-transfected group by two-tailed unpaired t-test), and DN-Cul4a- or DN-Cul4b-expressing PC12 cells (K). (n = 4; *p < 0.05 to control group by two-tailed unpaired t-test). Data are represented as mean \pm SEM. (L) Schematic summary of CRL4-mediated Dcx regulation.

cytosolic expression of Cul4b in developing neurons. Although Cul4b-1 and -x1 are the primary products of *Cul4b* in the adult brain, as previously reported,³⁹ Cul4b-x2, lacking the NLS-bearing N-terminus, appears to be responsible for the cytosolic function of Cul4b. When ectopically expressed, Cul4b-x2 primarily localizes to the cytosol, unlike other isoforms, and its mRNA and protein levels exhibit transient expression in developing neurons. Cell type- and time-specific alternative splicing is involved in neuronal differentiation, neuritic outgrowth, and synaptic formation during brain development.⁴⁰ For example, the pre-mRNA of postsynaptic density protein 95 undergoes splicing-dependent decay by timely expression of polypyrimidine tract-binding proteins, Ptbp1 and Ptbp2, in the early neurodevelopmental stage.³⁹ Consequently, we hypothesize that Cul4b pre-mRNA may be post-transcriptionally regulated by stage-specific alternative splicing during neurodevelopment. Furthermore, we demonstrated that the neddylation of Cul4a and Cul4b was transiently enhanced in developing neurons. Liu et al. reported that Cul4b-x2 is more neddylated than Cul4b-1 and Cul4b-x1 in the adult mouse brain; however, its expression is the lowest.³⁹ These results suggest that cytosolic CRL4 is highly functional during the early neurodevelopmental stage.

Neuronal activity is essential for neuronal development, survival, maturation, synaptic plasticity, and regeneration.^{18,19} Our results revealed that NMDA-induced neuronal activation downregulates CRL4 activity in mature neurons but not in immature neurons. Specifically,

NMDAR-mediated cation influx significantly reduced the neddylation of Cul4a and Cul4b. Consistently, the neddylation levels of Cul4a and Cul4b are lower in mature neurons than that in immature neurons. This process may result from the inhibition of neddylation proteins, such as Nae1, or the activation of deneddylating molecules, such as the Cop9 signalosome and cullin-associated NEDD8-dissociated protein 1.⁹ While there is no direct evidence of a molecular link between NMDA signaling and CRL neddylation, previous studies may provide some insight into this issue. Intracellular calcium influx can activate the NF- κ B signaling pathway in response to NMDA-induced excitotoxicity.^{41,42} Zhang et al. demonstrated that Csn5 is activated via phosphorylation by the IKK complex, an NF- κ B signaling molecule.⁴³ These findings suggest that NMDA-mediated calcium signaling likely inhibits CRL neddylation; however, further research is warranted to validate this possibility. Additionally, our data demonstrated that glutamate/NMDA stimulation induces nuclear accumulation of Cul4a in mature neurons, reducing its cytosolic localization. Thus, our findings suggest that the cytosolic function of Cul4a is downregulated under neuronal stimulation. Conversely, the nuclear accumulation of Cul4a may play a role in the protective response against DNA damage. For instance, upon UV exposure, the Cul4a-Ddb1 and/or Cul4b-Ddb1 complex is recruited to damaged DNA foci of the nucleus by Ddb2. Ddb2 recognizes several substrates, including histone H2A, for nucleotide excision repair and has other DNA damage responses as a DCAF.⁴⁴ Similarly, Cul4a is translocated into the nucleus and inhibits Parp1-mediated cell death under oxidative stress.⁴⁵ In neurons, glutamate/NMDA stimulation can also induce DNA damage, such as oxidation and single/double-strand breakage, resulting in activity-induced gene expression or neurodegeneration.^{46,47} Moreover, the Cul4a-Ddb1-Ddb2 complex is involved in base excision repair of oxidized DNA.⁴⁸ Therefore, glutamate/NMDA-induced nuclear accumulation of the Cul4a-Ddb1 complex may contribute to protective repair mechanisms against DNA damage. Collectively, we imply that CRL4 may function differently in the cytosol and nucleus under neuronal stimulation.

In this study, we first identified CRL4-interacting proteins in neurons. Despite using different experimental models, 29 of the 67 potential interactors have already been proposed as Cul4a- or Cul4b-interacting proteins according to open-source interactome data⁴⁹ (Table S1). This indicates that our experiment is reliable and that the interaction may be independent of cell type.

Cytoskeletal constituents such as actin, tubulin, and spectrin; cytoskeleton-regulating proteins, including Dcx, Dbn1, and Tmod2; and motor proteins, such as Myo5a, Myh10, and Spire1, are highly associated with CRL4, particularly with the cytosolic expression of Cul4a and Cul4b. Furthermore, on DIV10, RNA/DNA-binding molecules such as Tdp-43, Hnrmpd, Hnrmpf, Hnrnpg, Hnrnpk, Hnrnpl, Macroh2a2, Edf1a1, Ifl2, and Ell, as well as mitochondrial proteins such as Pdha1, Sucla2, Acat1, Atp5f1a, Uqcrc2, Slc25a3-4, Ywhaz, and Pck2, were identified as Cul4a- and Cul4b-interactors, in addition to cytoskeleton-regulating proteins. Considering that Cul4b is involved in dendritic spine formation in hippocampal neurons,¹⁶ our findings suggest that CRL4 may play a versatile role in mature neurons.

Our results also indicate that cytosolic CRL4 functions as a negative regulator of neurite morphogenesis. Genetic perturbation of Cul4a, which predominantly localizes to the cytosol, has a more pronounced effect on neurite extension and branching than nucleus-enriched Cul4b. However, Cul4b exhibits a similar inhibitory effect against NMDA-induced axonal extension upon NMDA treatment as Cul4a, which may result from the upregulation of its neddylation by NMDA. Considering that NMDA does not affect the expression and neddylation of Cul4a or Cul4b in immature neurons (DIV5), CRL4 appears to work antagonistically and/or independently to NMDA in axonal morphogenesis. Based on our data, CRL4 dysfunction could induce deregulated hyper-extension or over-sprouting of axons. However, axonal morphological defects have not been reported in *Cul4a*, *Cul4b*, or *Ddb1* knockout mice.^{16,50–54} Cul4b has even been identified as a positive regulator of neuronal differentiation.^{16,55} Nuclear Cul4b mediates NGF-induced neurite formation in PC12 cells by downregulating Wdr5, which epigenetically silences neuronal genes as a core subunit of the histone H3 lysine 4 methyltransferase complex.⁵⁵ Additionally, *Cul4b*-knockout male mice consistently exhibit a significant X-linked intellectual disability phenotype, owing to reduced dendrite complexity and spine density in hippocampal neurons.¹⁶ However, *Cul4a*-knockout mice exhibit no intellectual disability phenotype or neurological defects.⁵⁰ These reports imply a specific “neurogenic” function of nucleus-localizing Cul4b in the nervous system. Therefore, we suggest that the inconsistency between our study and previous studies may result from the differential function of nuclear Cul4b-scaffolded CRL4 vs. stage-specific cytosolic Cul4a/Cul4b-scaffolded CRL4 in neuritogenesis.

Similar to *CUL4B*, human *DCX* mutations have been linked to X-linked intellectual disability and epilepsy.⁵⁶ As CRL4 regulates the stability of Dcx, CRL4, and Dcx may share the same neuritogenesis signaling pathway. Dcx is also controlled by other E3 ligases. Mdm2 restricts the level of Dcx via the ubiquitination–proteasome degradation system, thereby inhibiting dendritic spine morphogenesis in olfactory bulb interneurons.³¹ Kihl15-CRL3 complex targets Dcx, resulting in the restriction of neuritogenesis.¹³ This implies that CRL3 and CRL4 may share substrates and have overlapping functions in neuritogenesis. Keap1-guided CRL3 and Wdr23-guided CRL4 independently target Nrf2, a transcription factor that mediates the stress response.⁵⁷ Furthermore, Crbn-bound CRL4 and Fbxo7-bound CRL1 inhibit voltage- and calcium-activated big-conductance potassium channels via ubiquitination.⁵⁸ These reports suggest that CRLs may have reciprocal and complementary functions, suggesting that inhibiting CRL4 alone may not be sufficient to induce neurodevelopmental defects, as Dcx can be ubiquitinated by other CRLs or E3 ligases. In addition, we found that immunoblot of Cul4a-immunoprecipitated Dcx shows slower mobility on SDS-PAGE gel in developing neuron (DIV4) than that of Cul4b-immunoprecipitated Dcx (Figure 8A). Thus, we postulated that Cul4a-immunoprecipitated Dcx may be highly post-translationally modified. Previous studies have demonstrated that the function, intracellular location, and protein stability of Dcx are regulated via phosphorylation in multiple serine/threonine sites by various kinases including cyclin-dependent kinase-5,^{59–61} c-Jun N-terminal kinase,⁶² protein kinase A,⁶³ microtubule affinity-regulating kinase,⁶³ rho kinase,⁶⁴ and glycogen synthase kinase 3 β ,⁶⁵ as well as in tyrosine site by tyrosine kinase such as Abelson tyrosine-protein kinase 1 (Abl1).⁶⁶ These processes regulate neurite extension, neuronal migration, axo/dendritogenesis, and spinogenesis. Especially in developing brains and neurons, the phosphorylated Dcx is highly enriched, resulting in slow mobility of the immunoblot of Dcx on SDS-PAGE gel, but it decreases in mature neurons.^{60,62,63} Based on these reports, we carefully presumed

that Cul4a may have a higher binding tendency with phosphorylated Dcx, but Cul4b may be prone to bind with dephosphorylated Dcx. We previously demonstrated that Abl1-mediated phosphorylation contributes to enhanced stability of Dcx protein.⁶⁶ It implies that the status of Dcx phosphorylation may be implicated in differential association with some E3 ligases, such as CRL4. However, this issue should be further investigated.

DCAFs involved in neurodevelopment, neurophysiology, and neuropathology remain largely unknown. CRL4 has been proposed as a platform for proteolysis-targeting chimera protein degraders that remove aberrant or toxic proteins via chemical-linked ubiquitination.⁶⁷ Further studies on neuronal DCAFs may provide novel strategies for addressing neurological disorders and neurodegenerative diseases.

Limitations of the study

First, the reliance on cultured neurons, while a valuable model, may limit the extrapolation of findings to *in vivo* conditions with their complex cellular interactions. Moreover, the study primarily focuses on the CRL4-Crbn-Dcx pathway. CRL4 also associates with other DCAFs, and more than 60 DCAFs have been identified.⁶⁸ Differential association with DCAF extensively differentiates the functionality of CRL4. Crbn, as a type of DCAF, has multiple endogenous substrates as well as Dcx, and it also can associate with neo-substrates linked by immunomodulatory drugs, including Thalidomide and its derivatives.⁶⁹ Therefore, further functional validation and exploration of CRL4-Crbn's implications for neuronal development are necessary. Second, our screening of the CRL4-binding partner seems to be biased on quantitatively enriched or stably associated proteins like cytoskeletal proteins because it was performed by the traditional immunoprecipitation method without additional depletion of highly enriched proteins or enrichment of transiently associating molecules. Recently, to overcome these technical flaws, protein-proximity labeling using BioID or APEX has been developed to explore protein-protein interaction.⁷⁰ This technique can be helpful in discovering a neuron-specific substrate and/or DCAFs of CRL4 for further study. Finally, acknowledging technical limitations and potential artifacts affecting the experimental procedures would provide a more comprehensive understanding of the research's scope and implications.

STAR★METHODS

Detailed methods are provided in the online version of this paper and include the following:

- KEY RESOURCES TABLE
- RESOURCE AVAILABILITY
 - Lead contact
 - Material availability
 - Data and code availability
- EXPERIMENTAL MODEL AND STUDY PARTICIPANT DETAILS
 - Animals
 - Rat primary cerebral neuron culture
 - PC12 cell culture
 - HEK293T cell culture
- METHOD DETAILS
 - Immunoblotting
 - Immunocytochemistry and proximity ligation assay
 - Immunohistochemistry
 - Fractionation of nucleus and cytosol
 - Immunoprecipitation
 - LC-MS/MS
 - DNA constructs
 - Gene transfection
 - Quantification of mRNA level
 - Quantification of neurite morphology
- QUANTIFICATION AND STATISTICAL ANALYSIS

SUPPLEMENTAL INFORMATION

Supplemental information can be found online at <https://doi.org/10.1016/j.isci.2024.108933>.

ACKNOWLEDGMENTS

We thank Mr. Kwangsoo Kim for his statistical advice and analysis. This work was supported by the DGIST R&D Program of the Ministry of Science and ICT (23-BT-06) and the National Research Foundation of Korea (NRF) Grant funded by the Korean Government (MSIP) (2020R1A2C2005174). It was also supported by the Basic Science Research Program of the NRF, funded by the Ministry of Education (2020R1A6A1A03040516).

AUTHOR CONTRIBUTIONS

Conceptualization, B.C. and C.M.; Methodology, T.S. and B.C.; Validation, T.S. and B.C.; Formal analysis, T.S. and B.C.; Investigation, T.S., B.C., J.Y.K., and W.C.K.; Resources, B.C., Y.-I.L., and C.M.; Data curation, T.S. and B.C.; Writing – Original Draft, T.S. and B.C.; Writing – Review and Editing, T.S., B.C., Y.-I.L., and C.M.; Visualization, T.S. and B.C.; Supervision, C.M.; Project administration, B.C. and C.M.; Funding acquisition, B.C. and C.M.

DECLARATION OF INTERESTS

The authors declare no competing interests.

Received: September 15, 2022

Revised: October 30, 2023

Accepted: January 12, 2024

Published: January 17, 2024

REFERENCES

1. Tau, G.Z., and Peterson, B.S. (2010). Normal development of brain circuits. *Neuropsychopharmacology* 35, 147–168.
2. Prem, S., Millonig, J.H., and DiCicco-Bloom, E. (2020). Dysregulation of Neurite Outgrowth and Cell Migration in Autism and Other Neurodevelopmental Disorders. *Adv. Neurobiol.* 25, 109–153.
3. Dogterom, M., and Koenderink, G.H. (2019). Actin-microtubule crosstalk in cell biology. *Nat. Rev. Mol. Cell Biol.* 20, 38–54.
4. Menon, S., and Gupton, S.L. (2016). Building Blocks of Functioning Brain: Cytoskeletal Dynamics in Neuronal Development. *Int. Rev. Cell Mol. Biol.* 322, 183–245.
5. Pimm, M.L., and Henty-Ridilla, J.L. (2021). New twists in actin-microtubule interactions. *Mol. Biol. Cell* 32, 211–217.
6. Lasser, M., Tiber, J., and Lowery, L.A. (2018). The Role of the Microtubule Cytoskeleton in Neurodevelopmental Disorders. *Front. Cell. Neurosci.* 12, 165.
7. Obin, M., Mesco, E., Gong, X., Haas, A.L., Joseph, J., and Taylor, A. (1999). Neurite outgrowth in PC12 cells. Distinguishing the roles of ubiquitylation and ubiquitin-dependent proteolysis. *J. Biol. Chem.* 274, 11789–11795.
8. Bryan, B., Cai, Y., Wrighton, K., Wu, G., Feng, X.H., and Liu, M. (2005). Ubiquitination of RhoA by Smurf1 promotes neurite outgrowth. *FEBS Lett.* 579, 1015–1019.
9. Hannah, J., and Zhou, P. (2015). Distinct and overlapping functions of the cullin E3 ligase scaffolding proteins CUL4A and CUL4B. *Gene* 573, 33–45.
10. Harper, J.W., and Schulman, B.A. (2021). Cullin-RING Ubiquitin Ligase Regulatory Circuits: A Quarter Century Beyond the F-Box Hypothesis. *Annu. Rev. Biochem.* 90, 403–429.
11. Amar, M., Pramod, A.B., Yu, N.K., Herrera, V.M., Qiu, L.R., Moran-Losada, P., Zhang, P., Trujillo, C.A., Ellegood, J., Urresti, J., et al. (2021). Autism-linked Cullin3 germline haploinsufficiency impacts cytoskeletal dynamics and cortical neurogenesis through RhoA signaling. *Mol. Psychiatry* 26, 3586–3613.
12. Morandell, J., Schwarz, L.A., Basilico, B., Tasciyan, S., Dimchev, G., Nicolas, A., Sommer, C., Kreuzinger, C., Dotter, C.P., Knaus, L.S., et al. (2021). Cul3 regulates cytoskeleton protein homeostasis and cell migration during a critical window of brain development. *Nat. Commun.* 12, 3058.
13. Song, J., Merrill, R.A., Usachev, A.Y., and Strack, S. (2021). The X-linked intellectual disability gene product and E3 ubiquitin ligase KLHL15 degrades doublecortin proteins to constrain neuronal dendritogenesis. *J. Biol. Chem.* 296, 100082.
14. Tarpey, P.S., Raymond, F.L., O’Meara, S., Edkins, S., Teague, J., Butler, A., Dicks, E., Stevens, C., Tofts, C., Avis, T., et al. (2007). Mutations in CUL4B, which encodes a ubiquitin E3 ligase subunit, cause an X-linked mental retardation syndrome associated with aggressive outbursts, seizures, relative macrocephaly, central obesity, hypogonadism, pes cavus, and tremor. *Am. J. Hum. Genet.* 80, 345–352.
15. Zou, Y., Liu, Q., Chen, B., Zhang, X., Guo, C., Zhou, H., Li, J., Gao, G., Guo, Y., Yan, C., et al. (2007). Mutation in CUL4B, which encodes a member of cullin-RING ubiquitin ligase complex, causes X-linked mental retardation. *Am. J. Hum. Genet.* 80, 561–566.
16. Chen, C.Y., Tsai, M.S., Lin, C.Y., Yu, I.S., Chen, Y.T., Lin, S.R., Juan, L.W., Chen, Y.T., Hsu, H.M., Lee, L.J., and Lin, S.W. (2012). Rescue of the genetically engineered Cul4b mutant mouse as a potential model for human X-linked mental retardation. *Hum. Mol. Genet.* 21, 4270–4285.
17. Schwechheimer, C. (2018). NEDD8-its role in the regulation of Cullin-RING ligases. *Curr. Opin. Plant Biol.* 45, 112–119.
18. Ewald, R.C., and Cline, H.T. (2009). NMDA Receptors and Brain Development. In *Biology of the NMDA Receptor*, A.M. Van Dongen, ed. (CRC Press/Taylor & Francis).
19. Kirischuk, S., Sinning, A., Blanquie, O., Yang, J.W., Luhmann, H.J., and Kilb, W. (2017). Modulation of Neocortical Development by Early Neuronal Activity: Physiology and Pathophysiology. *Front. Cell. Neurosci.* 11, 379.
20. Wilson, C., Rozés-Salvador, V., and Cáceres, A. (2020). Protocol for Evaluating Neuronal Polarity in Murine Models. *STAR Protoc.* 1, 100114.
21. Jin, J., Ang, X.L., Shirogane, T., and Wade Harper, J. (2005). Identification of substrates for F-box proteins. *Methods Enzymol.* 399, 287–309.
22. Lee, L.J., Lo, F.S., and Erzurumlu, R.S. (2005). NMDA receptor-dependent regulation of axonal and dendritic branching. *J. Neurosci.* 25, 2304–2311.
23. Wang, Y., Tang, J.L., Xu, X., Zhou, X.P., Du, J., Wang, X., Zhou, Y., Zhu, Q., Yao, L.L., Wang, Y.G., et al. (2018). NMDA receptors inhibit axonal outgrowth by inactivating Akt and activating GSK-3beta via calcineurin in cultured immature hippocampal neurons. *Exp. Cell Res.* 371, 389–398.
24. George, J., Dravid, S.M., Prakash, A., Xie, J., Peterson, J., Jabba, S.V., Baden, D.G., and Murray, T.F. (2009). Sodium channel activation augments NMDA receptor function and promotes neurite outgrowth in immature cerebrocortical neurons. *J. Neurosci.* 29, 3288–3301.
25. George, J., Baden, D.G., Gerwick, W.H., and Murray, T.F. (2012). Bidirectional influence of sodium channel activation on NMDA receptor-dependent cerebrocortical neuron structural plasticity. *Proc. Natl. Acad. Sci. USA* 109, 19840–19845.
26. Choi, D.W., Maulucci-Gedde, M., and Kriegstein, A.R. (1987). Glutamate neurotoxicity in cortical cell culture. *J. Neurosci.* 7, 357–368.
27. Francis, F., Koulakoff, A., Boucher, D., Chafey, P., Schaar, B., Vinet, M.C., Friocourt, G., McDonnell, N., Reiner, O., Kahn, A., et al. (1999). Doublecortin is a developmentally regulated, microtubule-associated protein expressed in migrating and differentiating neurons. *Neuron* 23, 247–256.
28. Horesh, D., Sapir, T., Francis, F., Wolf, S.G., Caspi, M., Elbaum, M., Chelly, J., and Reiner, O. (1999). Doublecortin, a stabilizer of microtubules. *Hum. Mol. Genet.* 8, 1599–1610.
29. Cohen, D., Segal, M., and Reiner, O. (2008). Doublecortin supports the development of dendritic arbors in primary hippocampal neurons. *Dev. Neurosci.* 30, 187–199.
30. Fu, X., Brown, K.J., Yap, C.C., Winckler, B., Jaiswal, J.K., and Liu, J.S. (2013). Doublecortin (Dcx) family proteins regulate filamentous actin structure in developing neurons. *J. Neurosci.* 33, 709–721.
31. Yoshihara, S.I., Takahashi, H., Nishimura, N., Kinoshita, M., Asahina, R., Kitsuki, M., Tatsumi, K., Furukawa-Hibi, Y., Hirai, H., Nagai, T., et al. (2014). Npas4 regulates Mdm2 and thus Dcx in experience-dependent dendritic spine development of newborn olfactory bulb interneurons. *Cell Rep.* 8, 843–857.
32. Wiatrak, B., Kubis-Kubiak, A., Piwowar, A., and Barg, E. (2020). PC12 Cell Line: Cell Types, Coating of Culture Vessels, Differentiation and Other Culture Conditions. *Cells* 9, 958.

33. Cornell, B., Wachi, T., Zhukarev, V., and Toyooka, K. (2016). Regulation of neuronal morphogenesis by 14-3-3epsilon (Ywhae) via the microtubule binding protein, doublecortin. *Hum. Mol. Genet.* 25, 4610.
34. Uhlén, M., Fagerberg, L., Hallström, B.M., Lindskog, C., Oksvold, P., Mardinoglu, A., Sivertsson, Å., Kampf, C., Sjöstedt, E., Asplund, A., et al. (2015). Proteomics. Tissue-based map of the human proteome. *Science* 347, 1260419.
35. Thul, P.J., Åkesson, L., Wiking, M., Mahdessian, D., Geladaki, A., Ait Blal, H., Alm, T., Asplund, A., Björk, L., Breckels, L.M., et al. (2017). A subcellular map of the human proteome. *Science* 356, eaal3321.
36. Higgins, J.J., Pucilowska, J., Lombardi, R.Q., and Rooney, J.P. (2004). A mutation in a novel ATP-dependent Lon protease gene in a kindred with mild mental retardation. *Neurology* 63, 1927–1931.
37. Higgins, J.J., Tal, A.L., Sun, X., Hauck, S.C.R., Hao, J., Kosofosky, B.E., and Rajadhyaksha, A.M. (2010). Temporal and spatial mouse brain expression of cereblon, an ionic channel regulator involved in human intelligence. *J. Neurogenet.* 24, 18–26.
38. Nekooki-Machida, Y., and Hagiwara, H. (2020). Role of tubulin acetylation in cellular functions and diseases. *Med. Mol. Morphol.* 53, 191–197.
39. Liu, H.C., Enikolopov, G., and Chen, Y. (2012). Cul4B regulates neural progenitor cell growth. *BMC Neurosci.* 13, 112.
40. Su, C.H., D, D., and Tarn, W.Y. (2018). Alternative Splicing in Neurogenesis and Brain Development. *Front. Mol. Biosci.* 5, 12.
41. Shen, W.H., Zhang, C.Y., and Zhang, G.Y. (2003). Modulation of IκappaB kinase autophosphorylation and activity following brain ischemia. *Acta Pharmacol. Sin.* 24, 311–315.
42. Caba, E., and Bahr, B.A. (2004). Biphasic NF-kappaB activation in the excitotoxic hippocampus. *Acta Neuropathol.* 108, 173–182.
43. Zhang, J., Zhao, R., Yu, C., Bryant, C.L.N., Wu, K., Liu, Z., Ding, Y., Zhao, Y., Xue, B., Pan, Z.-Q., et al. (2020). IKK-Mediated Regulation of the COP9 Signalosome via Phosphorylation of CSN5. *J. Proteome Res.* 19, 1119–1130.
44. Kapetanaki, M.G., Guerrero-Santoro, J., Bisi, D.C., Hsieh, C.L., Rapić-Otrin, V., and Levine, A.S. (2006). The DDB1-CUL4ADDB2 ubiquitin ligase is deficient in xeroderma pigmentosum group E and targets histone H2A at UV-damaged DNA sites. *Proc. Natl. Acad. Sci. USA* 103, 2588–2593.
45. Ye, N., Zhang, N., Zhang, Y., Qian, H., Wu, B., and Sun, Y. (2019). Cul4a as a New Interaction Protein of PARP1 Inhibits Oxidative Stress-Induced H9c2 Cell Apoptosis. *Oxid. Med. Cell. Longev.* 2019, 4273261.
46. Madabhushi, R., Pan, L., and Tsai, L.H. (2014). DNA damage and its links to neurodegeneration. *Neuron* 83, 266–282.
47. Caldecott, K.W., Ward, M.E., and Nussenzweig, A. (2022). The threat of programmed DNA damage to neuronal genome integrity and plasticity. *Nat. Genet.* 54, 115–120.
48. Kumar, N., Theil, A.F., Roginskaya, V., Ali, Y., Calderon, M., Watkins, S.C., Barnes, R.P., Opresko, P.L., Pines, A., Lans, H., et al. (2022). Global and transcription-coupled repair of 8-oxoG is initiated by nucleotide excision repair proteins. *Nat. Commun.* 13, 974.
49. Stark, C., Breikreutz, B.J., Reguly, T., Boucher, L., Breikreutz, A., and Tyers, M. (2006). BioGRID: a general repository for interaction datasets. *Nucleic Acids Res.* 34, D535–D539.
50. Liu, L., Lee, S., Zhang, J., Peters, S.B., Hannah, J., Zhang, Y., Yin, Y., Koff, A., Ma, L., and Zhou, P. (2009). CUL4A abrogation augments DNA damage response and protection against skin carcinogenesis. *Mol. Cell* 34, 451–460.
51. Kopanja, D., Roy, N., Stoyanova, T., Hess, R.A., Bagchi, S., and Raychaudhuri, P. (2011). Cul4A is essential for spermatogenesis and male fertility. *Dev. Biol.* 352, 278–287.
52. Yin, Y., Lin, C., Kim, S.T., Roig, I., Chen, H., Liu, L., Veith, G.M., Jin, R.U., Keeney, S., Jasin, M., et al. (2011). The E3 ubiquitin ligase Cullin 4A regulates meiotic progression in mouse spermatogenesis. *Dev. Biol.* 356, 51–62.
53. Jiang, B., Zhao, W., Yuan, J., Qian, Y., Sun, W., Zou, Y., Guo, C., Chen, B., Shao, C., and Gong, Y. (2012). Lack of Cul4b, an E3 ubiquitin ligase component, leads to embryonic lethality and abnormal placental development. *PLoS One* 7, e37070.
54. Cang, Y., Zhang, J., Nicholas, S.A., Bastien, J., Li, B., Zhou, P., and Goff, S.P. (2006). Deletion of DDB1 in mouse brain and lens leads to p53-dependent elimination of proliferating cells. *Cell* 127, 929–940.
55. Nakagawa, T., and Xiong, Y. (2011). X-linked mental retardation gene CUL4B targets ubiquitylation of H3K4 methyltransferase component WDR5 and regulates neuronal gene expression. *Mol. Cell* 43, 381–391.
56. Gleeson, J.G., Allen, K.M., Fox, J.W., Lamperti, E.D., Berkovic, S., Scheffer, I., Cooper, E.C., Dobyns, W.B., Minnerath, S.R., Ross, M.E., and Walsh, C.A. (1998). Doublecortin, a brain-specific gene mutated in human X-linked lissencephaly and double cortex syndrome, encodes a putative signaling protein. *Cell* 92, 63–72.
57. Lo, J.Y., Spatola, B.N., and Curran, S.P. (2017). WDR23 regulates NRF2 independently of KEAP1. *PLoS Genet.* 13, e1006762.
58. Song, T., Liang, S., Liu, J., Zhang, T., Yin, Y., Geng, C., Gao, S., Feng, Y., Xu, H., Guo, D., et al. (2018). CRL4 antagonizes SCFFbxo7-mediated turnover of cereblon and BK channel to regulate learning and memory. *PLoS Genet.* 14, e1007165.
59. Graham, M.E., Ruma-Haynes, P., Capes-Davis, A.G., Dunn, J.M., Tan, T.C., Valova, V.A., Robinson, P.J., and Jeffrey, P.L. (2004). Multisite phosphorylation of doublecortin by cyclin-dependent kinase 5. *Biochem. J.* 381, 471–481.
60. Tanaka, T., Serneo, F.F., Tseng, H.C., Kulkarni, A.B., Tsai, L.H., and Gleeson, J.G. (2004). Cdk5 phosphorylation of doublecortin ser297 regulates its effect on neuronal migration. *Neuron* 41, 215–227.
61. Moslehi, M., Ng, D.C.H., and Bogoyevitch, M.A. (2019). Doublecortin X (DCX) serine 28 phosphorylation is a regulatory switch, modulating association of DCX with microtubules and actin filaments. *Biochim. Biophys. Acta. Mol. Cell Res.* 1866, 638–649.
62. Gdalyahu, A., Ghosh, I., Levy, T., Sapir, T., Sapoznik, S., Fishler, Y., Azoulai, D., and Reiner, O. (2004). DCX, a new mediator of the JNK pathway. *EMBO J.* 23, 823–832.
63. Schaar, B.T., Kinoshita, K., and McConnell, S.K. (2004). Doublecortin microtubule affinity is regulated by a balance of kinase and phosphatase activity at the leading edge of migrating neurons. *Neuron* 41, 203–213.
64. Amano, M., Tsumura, Y., Taki, K., Harada, H., Mori, K., Nishioka, T., Kato, K., Suzuki, T., Nishioka, Y., Iwamoto, A., and Kaibuchi, K. (2010). A proteomic approach for comprehensively screening substrates of protein kinases such as Rho-kinase. *PLoS One* 5, e8704.
65. Bilimoria, P.M., de la Torre-Ubieta, L., Ikeuchi, Y., Becker, E.B.E., Reiner, O., and Bonni, A. (2010). A JIP3-regulated GSK3beta/DCX signaling pathway restricts axon branching. *J. Neurosci.* 30, 16766–16776.
66. Kim, J.Y., Cho, B., and Moon, C. (2020). Timely Inhibitory Circuit Formation Controlled by Abl1 Regulates Innate Olfactory Behaviors in Mouse. *Cell Rep.* 30, 187–201.e4.
67. Békés, M., Langley, D.R., and Crews, C.M. (2022). PROTAC targeted protein degraders: the past is prologue. *Nat. Rev. Drug Discov.* 21, 181–200.
68. Lee, J., and Zhou, P. (2007). DCAF6, the missing link of the CUL4-DDB1 ubiquitin ligase. *Mol. Cell* 26, 775–780.
69. Kim, H.K., Seol, J.E., Ahn, S.W., Jeon, S., Park, C.S., and Han, J. (2021). Cereblon: promise and challenges for combating human diseases. *Pflugers Arch.* 473, 1695–1711.
70. Qin, W., Cho, K.F., Cavanagh, P.E., and Ting, A.Y. (2021). Deciphering molecular interactions by proximity labeling. *Nat. Methods* 18, 133–143.
71. Kolberg, L., Raudvere, U., Kuzmin, I., Adler, P., Vilo, J., and Peterson, H. (2023). g:Profiler-interoperable web service for functional enrichment analysis and gene identifier mapping (2023 update). *Nucleic Acids Res.* 51, W207–W212.
72. Fredriksson, S., Gullberg, M., Jarvius, J., Olsson, C., Pietras, K., Gústafsdóttir, S.M., Ostman, A., and Landegren, U. (2002). Protein detection using proximity-dependent DNA ligation assays. *Nat. Biotechnol.* 20, 473–477.
73. Hu, J., Zacharek, S., He, Y.J., Lee, H., Shumway, S., Duronio, R.J., and Xiong, Y. (2008). WD40 protein FBW5 promotes ubiquitination of tumor suppressor TSC2 by DDB1-CUL4-ROC1 ligase. *Genes Dev.* 22, 866–871.
74. Welm, B.E., Dijkgraaf, G.J.P., Bledau, A.S., Welm, A.L., and Werb, Z. (2008). Lentiviral transduction of mammary stem cells for analysis of gene function during development and cancer. *Cell Stem Cell* 2, 90–102.
75. Heckl, D., Kowalczyk, M.S., Yudovich, D., Belzair, R., Puram, R.V., McConkey, M.E., Thielke, A., Aster, J.C., Regev, A., and Ebert, B.L. (2014). Generation of mouse models of myeloid malignancy with combinatorial genetic lesions using CRISPR-Cas9 genome editing. *Nat. Biotechnol.* 32, 941–946.
76. Labun, K., Montague, T.G., Krause, M., Torres Cleuren, Y.N., Tjeldnes, H., and Valen, E. (2019). CHOPCHOP v3: expanding the CRISPR web toolbox beyond genome editing. *Nucleic Acids Res.* 47, W171–W174.
77. Arshadi, C., Günther, U., Eddison, M., Harrington, K.I.S., and Ferreira, T.A. (2021). SNT: a unifying toolbox for quantification of neuronal anatomy. *Nat. Methods* 18, 374–377.

STAR★METHODS

KEY RESOURCES TABLE

REAGENT or RESOURCE	SOURCE	IDENTIFIER
Antibodies		
Rabbit polyclonal anti-Cul4a	Abcam	Cat# ab72548; RRID:AB_1268363
Rabbit polyclonal anti-Cul4b	Proteintech	Cat# 12916-1-AP; RRID:AB_2086699
Goat polyclonal anti-Ddb1	Abcam	Cat# ab9194, RRID:AB_307063
Mouse monoclonal anti-Actin (C4)	EMD Millipore Corporation	Cat# MAB1501; RRID:AB_2223041
Rabbit polyclonal anti-Lmnb1	Abcam	Cat# ab16048; RRID:AB_443298
Mouse monoclonal anti-Dcx (E-6)	Santa Cruz Biotechnology	Cat# sc-271390; RRID:AB_10610966
Mouse monoclonal anti-acetylated α -tubulin (6-11B-1)	Santa Cruz Biotechnology	Cat# sc-23950; RRID:AB_628409
Mouse monoclonal anti-mCherry (1C51)	Abcam	Cat# ab125096; RRID:AB_11133266
Mouse monoclonal anti-Flag	Sigma-Aldrich	Cat# F1804; RRID:AB_262044
Chicken polyclonal anti-Tau	Abcam	Cat# ab75714; RRID:AB_1310734
Rabbit polyclonal anti-Crbn	Invitrogen	Cat# PA5-61122; RRID:AB_2640143
Mouse monoclonal anti-Myc (9E10)	Santa Cruz Biotechnology	Cat# sc-40; RRID:AB_627268
Mouse monoclonal anti-Ha (F-7)	Santa Cruz Biotechnology	Cat# sc-7392; RRID:AB_627809
Rabbit polyclonal anti-GFP	Invitrogen	Cat# A6455; RRID:AB_221570
Chemicals, peptides, and recombinant proteins		
Glutamate receptor antagonists (D-AP5, NBQX disodium salt, and LY341495 sodium salt)	Abcam	Cat# ab120376
Memantine	Abcam	Cat# ab146687
MLN4924	Abcam	Cat# ab216470
CSN5i-3	MedChemExpress	Cat# HY-112134
Alexa Flour 488 Phalloidin	Thermo Fisher Scientific	Cat# A12379
Critical commercial assays		
Duolink® <i>In Situ</i> Red Starter Kit Mouse/Rabbit	Sigma-Aldrich	Cat# DUO92101
Duolink® <i>In Situ</i> Orange Starter Kit Goat/Rabbit	Sigma-Aldrich	Cat# DUO92106
CalPhos Mammalian Transfection Kit	Clontech	Cat# 631312
Experimental models: Cell lines		
PC12 Cell Line	ATCC	Cat# CRL-1721
Rat primary cerebral neuron	This paper	N/A
HEK293T Cell Line	ATCC	Cat# CRL-3216
Experimental models: Organisms/strains		
Rat: Sprague Dawley	Korean Animal Technology (KOATECH)	N/A
Oligonucleotides		
Primers for cloning rCul4b isoforms, see Table S2	This paper	N/A
Oligonucleotides for inserting MCS in pcDNA3.2-V5-YFP, see Table S2	This paper	N/A
Primers for cloning rCrbn, see Table S2	This paper	N/A
Oligonucleotides for sgLacZ, sgCul4a, sgCul4b, and sgCrbn, see Table S2	This paper	N/A
Primers for quantifying mRNA level of rCul4a, rCul4b, rCul4b isoforms, and rPpia, see Table S2	This paper	N/A

(Continued on next page)

Continued

REAGENT or RESOURCE	SOURCE	IDENTIFIER
Recombinant DNA		
pHIV-EGFP	This paper	N/A
pHIV-DN-hCUL4A-FLAG-EGFP	This paper	N/A
pHIV-DN-hCUL4B-FLAG-EGFP	This paper	N/A
pCMV-Myc-rCul4b-1	This paper	N/A
pCMV-Myc-rCul4b-x1	This paper	N/A
pCMV-Myc-rCul4b-x2	This paper	N/A
pL-CRISPR-sgLacZ-GFP	This paper	N/A
pL-CRISPR-sgCul4a-GFP	This paper	N/A
pL-CRISPR-sgCul4b-GFP	This paper	N/A
pL-CRISPR-sgCrbn-GFP	This paper	N/A
Software and algorithms		
Fiji	NIH	https://imagej.nih.gov/ij/
Sigmaplot12.0	Systat Software Inc.	https://systatsoftware.com/
g:Profiler	Kolberg et al. ⁷¹	https://biit.cs.ut.ee/gprofiler/gost
Other		
Data S1, S2, S3, and S4	This paper	Mendeley Data, V1, https://doi.org/10.17632/tvh5nhwx3c.1 (https://data.mendeley.com/datasets/tvh5nhwx3c/1)

RESOURCE AVAILABILITY

Lead contact

Further information and requests for resources and reagents should be directed to and will be fulfilled by the Lead Contact, Bongki Cho (cbk34@dgist.ac.kr).

Material availability

This study did not generate new reagents. Plasmids generated in this study are available from the [lead contact](#) upon request.

Data and code availability

- LC_MS/MS raw data have been deposited at Mendeley Data and are publicly available as of the date of publication. Accession numbers are listed in the [key resources table](#). Original western blot images and microscopy data reported in this paper will be shared by the [lead contact](#) upon request.
- This study did not generate new code.
- Any additional information required to reanalyze the data reported in this paper is available from the [lead contact](#) upon request.

EXPERIMENTAL MODEL AND STUDY PARTICIPANT DETAILS

Animals

All animals were handled according to Laboratory Animal Resource Center and Daegu Gyeongbuk Institute of Science and Technology IACUC guidelines (Approval No. DGIST-IACUC-20102701-0000). All experimental protocols were approved by the Institutional Animal Care and Use Committees of DGIST. Sprague-Dawley rats were obtained from KOATECH (Korea).

Rat primary cerebral neuron culture

On rat embryonic day 18, the cerebral cortex was dissected in pre-chilled Hank's buffered salt solution (#14025, Gibco, Waltham, MA, USA), which is supplemented with 6% glucose (Sigma-Aldrich, St. Louis, MO, USA) and 50 unit per ml penicillin-streptomycin (#15140, Gibco, Waltham, MA, USA). The cerebral cortices were trypsinized and physically dissociated by pipetting into single neurons. The dissociated neurons were plated at a density of 1×10^5 cells per cm^2 onto glass coverslips, plates, or dishes which are pre-coated with poly-D-lysine (#P6407, Sigma-Aldrich, St. Louis, MO, USA) and fed in neurobasal media (#21103, Gibco, Waltham, MA, USA) containing 2% B27 supplement (#17504, Gibco,

Waltham, MA, USA), 0.5 mM L-glutamine (#25030, Gibco, Waltham, MA, USA) and 50 unit per ml penicillin/streptomycin. The neurons were incubated in 5% CO₂ at 37°C. And then, half of the medium was exchanged with fresh media per three days.

PC12 cell culture

PC12 cell line (#CRL-1721™) was purchased from ATCC (Manassas, VA, USA). PC12 cells were seeded on a 12-well or 6-well plate coated by poly D-lysine (0.01%; Sigma Chemical Co., USA) and grown in RPMI 1640 medium (#11875093, Gibco, USA) containing 10% horse serum (#26050088, Gibco, USA), 5% fetal bovine serum (FBS) (#SH30919.03, Hyclone, USA), and 1% penicillin/streptomycin at 37°C with 5% CO₂.

HEK293T cell culture

HEK293T cell line (#CRL-3216™) was purchased from ATCC (Manassas, VA, USA). HEK293T cells were seeded on a 6-well plate coated by poly D-lysine (0.01%; Sigma Chemical Co., USA) and grown in DMEM medium (#LM001-05, WELGENE, Gyeongsan, Korea) containing 10% fetal bovine serum (FBS) (#SH30919.03, Hyclone, USA), and 1% penicillin/streptomycin at 37°C with 5% CO₂.

METHOD DETAILS

Immunoblotting

Cultured cerebral neurons were collected in lysis buffer (125mM Tris-Cl, 4% SDS, pH6.8) with a protease and phosphatase inhibitor cocktail (#78442, ThermoFisher Scientific, Waltham, MA, USA). The protein concentration of the lysates was measured using a BCA assay (#23225, ThermoFisher Scientific, Waltham, MA, USA). And then, the lysates were loaded into SDS-PAGE and transferred into PVDF membrane (#IPVH00010, Millipore, Darmstadt, Germany). The membranes were blocked with 5% non-fat milk (#232100, BD, Franklin Lakes, NJ, USA) in TBST at room temperature for 1 h and treated by primary antibodies for over 2 h. After washing with TBST, HRP-conjugated antibodies were treated, washed with TBST, and immunoblotted using Pierce ECL western blotting substrate (#23225, ThermoFisher Scientific, Waltham, MA, USA).

Immunocytochemistry and proximity ligation assay

Cultured neurons were rinsed with PBS and fixed with 4% paraformaldehyde in PBS at room temperature for 15 min. After washing out with PBST (0.03% Triton X-100 in PBS), cells were incubated with a blocking solution (3% BSA in PBST) at room temperature for 30 min. The primary antibodies, diluted into a blocking solution with proper titer (1:100-200), were treated at room temperature for 2 h. After washing with PBST, fluorescence-conjugated secondary antibodies were diluted in a blocking solution (1:200) and treated for 1 h. The specimen was mounted onto slide glass with a DAPI-contained mounting solution (#H-1200, Vectashield, Burlingame, CA, USA). For proximity ligation assay,⁷² used Duolink® *In Situ* Orange Starter Kit according to manufacturer's protocol.

Immunohistochemistry

The Sprague-Dawley rats were anesthetized by using Zoletil 50 (Virbac, Carros, France) (50mg/kg) and Rompun (Bayer AG, Leverkusen, Germany) (5~10mg/kg), transcardially perfused with cold saline (0.9% NaCl), and fixed with pre-chilled 4% paraformaldehyde in PBS. Brain tissues were dissected, dehydrated by 2-h serial incubations with 70%, 85%, 95%, and 100% ethanol (#1.00983.1011, Merck, Darmstadt, Germany), soaked in xylene (#117, Duksan, Seoul, South Korea) for 4 h, and finally embedded into paraffin for 4 h. The paraffin-embedded samples were sectioned at five μm thickness by a rotary microtome (Leica, Buffalo Grove, IL, United States). The sections were attached to the micro slide glass (#BM5516, Muto Pure Chemicals, Tokyo, Japan). For antigen retrieval, they were treated with 0.01 M citric acid monohydrate (pH 6.0) at 100°C for 5 min and permeated in 3% hydrogen peroxide for 30 min. And then, they were incubated with blocking solution (5% normal donkey serum in PBST) at room temperature for 1 h and treated with primary antibodies, diluted in blocking solution, at 4°C for over 16 h. After several washes, secondary fluorescence-conjugated antibodies were treated for 1 h at room temperature and mounted with a DAPI-contained mounting solution.

Fractionation of nucleus and cytosol

Neurons were collected in pre-chilled fractionation buffer (250 mM sucrose, 10 mM KCl, 5 mM MgCl₂, 1 mM EDTA, 1 mM EGTA, 20 mM HEPES, protease and phosphatase inhibitor cocktails, pH7.5). The lysate was passed through a 27-gauge needle with a syringe 10-times and centrifuged at 500 ×g for 15 min at 4°C. The pellet containing the nucleus-enriched fraction and the supernatant containing the cytosolic fraction were separately collected. The pellet was resuspended into a fractionation buffer for nuclear-enriched fraction, passed through a 27-gauge needle, and centrifuged at 500 ×g for 15 min. And this process was repeated twice to clear residual other cellular compartments. The final pellet was lysed in lysis buffer (125 mM Tris-Cl, 4% SDS, pH6.8). For cytosolic fraction, the supernatant was centrifuged at 10000 ×g for 15 min at 4°C. The residual pellet, which contains a membrane-enriched fraction, was discarded, and the supernatant was resuspended into fractionation buffer and centrifuged at 10000 ×g for 15 min to wash other cellular compartments. This process was performed twice, and the final supernatant was lysed in lysis buffer.

Immunoprecipitation

Cultured neurons were lysed with immunoprecipitation buffer (100 mM NaCl, 5 mM EDTA, 50 mM Tris-Cl, and 0.5% Triton X-100, pH7.4) and passed through a 28-gauge needle with a syringe ten times to further lyse. The lysate was centrifuged at 13200 rpm at 4°C for 20 min, and its supernatant was collected. The lysate was pre-cleared with protein-A/G agarose beads (#20421, ThermoFisher Scientific, Waltham, MA, USA), and its protein amount was measured by BCA assay (#23225, ThermoFisher Scientific, Waltham, MA, USA). Primary antibodies were treated in the lysate with slow rotation at 4°C overnight. The next day, the protein-A/G agarose bead was incubated with the sample for 2 h, spun down at 2000 ×g for 3 min, and washed with immunoprecipitation buffer. The immunoreacting protein-A/G agarose bead was lysed with SDS loading buffer at 95°C for 10 min. And then, its supernatant was loaded with SDS-PAGE, and further experiments were performed.

LC-MS/MS

Nano LC-MS/MS analysis was performed with a nano HPLC system (Agilent, Wilmington, DE). The nanochip column (Agilent, Wilmington, DE, 43 mm × 0.075 mm) was used for peptide separation. Mobile phase A for LC separation was 0.1% formic acid in deionized water, and mobile phase B was 0.1% formic acid in acetonitrile. The chromatography gradient was designed for a linear increase from 3% B to 45% B in 30 min, 45% B to 95% B in 1 min, 95% B in 4 min, and 3% B in 10 min. The flow rate was maintained at 300 nl/min. Product ion spectra were collected in the information-dependent acquisition (IDA) mode and were analyzed by Agilent 6530 Accurate-Mass Q-TOF using continuous cycles of one full scan TOF MS from 300-2000 m/z (1.0 s) plus three product ion scans from 150-2000 m/z (1.5 s each). Precursor m/z values were selected starting with the most intense ion, using a selection quadrupole resolution of 3 Da. The rolling collision energy feature was used, which determines collision energy based on the precursor value and charge state. The dynamic exclusion time for precursor ion m/z values was 60 s.

The mascot algorithm (Matrixscience, USA) was used to identify peptide sequences in a protein sequence database. Database search criteria were taxonomy; Rattus (148853 sequences; 70437683 residues), fixed modification; carbamidomethylated at cysteine residues, variable modification; oxidized at methionine residues, maximum allowed missed cleavage; 2, MS tolerance; 100 ppm, MS/MS tolerance; 0.1 Da. Only peptides resulting from trypsin digests were considered. The peptides were filtered with a significance threshold of $p < 0.05$.

DNA constructs

For genetic perturbation of CRL4, pcDNA3-HA2-CUL4A, pcDNA3-myc3-CUL4B, and pcDNA3-HA2-DDB1 were gifts from Yue Xiong (Addgene plasmid #19907, #19922, #19909).⁷³ And pcDNA3-DN-hCUL4A-FLAG and pcDNA3-DN-hCUL4B-FLAG were gifts from Wade Harper (Addgene plasmid #15821, #15822).²¹ pHIV-EGFP was a gift from Bryan Welm & Zena Werb (Addgene plasmid #21373).⁷⁴ For DN-Cul4a and DN-Cul4b, we obtained blunt-ended PCR products from pcDNA3-DN-hCUL4A-FLAG or pcDNA3-DN-hCUL4B-FLAG and then inserted them into HpaI-digested pHIV-EGFP. Myc-tagged rat Cul4b-1, -x1, and -x2 isoforms were generated by inserting each PCR product into BamHI and XhoI of pcDNA3. The PCR products were obtained from the cDNA of rat-cultured cerebral neurons using DNA oligomers. For pcDNA-V5-tagged Crbn, the same cDNA of rat-cultured cerebral neurons was also used. The PCR product was subcloned into XhoI restriction enzyme site inserted pcDNA3.2-V5-DEST vector after digested with SacII and XhoI. For CRISPR-Cas9-mediated knockout of Cul4a, Cul4b, and Crbn, pL-CRISPR.EFS.GFP was a gift from Benjamin Ebert (Addgene plasmid # 57818).⁷⁵ The sgRNAs were designed from CHOPCHOP (version 3) (<https://chopchop.cbu.uib.no/>).⁷⁶ DNA oligomers containing the sgRNAs were annealed and inserted into BsmBI-digested pL-CRISPR.EFS.GFP.

Gene transfection

We used CalPhos Mammalian Transfection Kit (#631312, Clontech, Japan) for gene transfection into cultured neurons, according to the manufacturer's protocol. We transfected DNA clones into cultured neurons on DIV2 and fixed them on DIV4. Lipofectamine 3000 (#L3000001, Thermo Fisher Scientific, Waltham, MA, USA) was used for gene transfection into PC12 cells, according to the manufacturer's protocol.

Quantification of mRNA level

We extracted total RNA from cultured neurons using RNeasy Plus Mini Kit (#74136, Qiagen, Düsseldorf, Germany) and followed the manufacturer's protocol. The mRNA was reverse-transcribed to cDNA using SuperScript IV Reverse Transcriptase (#18090010, Thermo Fisher Scientific, Waltham, MA, USA). We performed PCR using Herculase II Fusion DNA Polymerase (#600677, Agilent, Santa Clara, CA, USA) with primers.

Quantification of neurite morphology

To quantify neurite morphology, we first fixed the cultured neurons expressing GFP on DIV4 with 4% paraformaldehyde in PBS, then enhanced the GFP signal by staining with anti-GFP. We obtained individual images of 50 or 100 neurons onto 2-3 coverslips (18 mm Φ) using a confocal inverted or upright laser-scanning microscope (LSM700 or LSM780, Carl Zeiss, Germany). Each neuronal morphology was semi-automatically traced and skeletonized using the Simple Neurite Tracer (SNT) plugin of the FIJI program (NIH, USA).⁷⁷ The SNT plugin calculated the number and length of total neurites and branches based on the neurite traces.

QUANTIFICATION AND STATISTICAL ANALYSIS

Statistic information is described in the figure legends. All experiments were performed at least three times from independent cell or animal preparations. Repeats for experiments or cell numbers are given in the figure legends as 'n.' Error bars represent \pm standard error (SEM). To measure statistical significance, we performed two-tailed unpaired t-test, Mann-Whitney rank sum test, and one-way ANOVA on ranks using Dunnett's Method. Throughout the study, $p < 0.05$ was considered significant. All statistical analyses and graph plotting were conducted by using the Sigmaplot12.0 program.